2012

Finite element analysis of stress distribution within metal-on-metal joint replacements

Yujing Liu
Edith Cowan University

Edith Cowan University

Copyright Warning

SCHOOL OF ENGINEERING

FACULTY OF COMPUTING, HEALTH AND SCIENCE

EDITH COWAN UNIVERSITY

Finite element analysis of stress distribution within metal-on-metal joint replacements

By

Yujing Liu

March 2012

This thesis is presented in fulfilment of the requirements for the degree of Master of Engineering Science

USE OF THESIS

The Use of Thesis statement is not included in this version of the thesis.

ABSTRACT

Demand for joint replacements is rising in Australia, driven by a sharp increase in the number of joint problems associated with population aging and obesity. In artificial joints, delamination or failure within the coatings occurs when the stress reaches a critical level, resulting in large wear debris particles appearing on the contact surface between the head and the cup.

The process has been described as due to a stress-corrosion-cracking mechanism. Under the same loading, stress increases when the contact area decreases, which happens in the vicinity of wear debris. As such, once wear debris is generated, a catastrophic process could be initiated, resulting in more stress-corrosion-cracking. As such, acquiring a strong coating that will not fail is highly desirable for the applications of hip joint replacement. Failure in a coating layer is normally initiated by excessive local tensile or shear stress; therefore, it is important to clarify the stress distribution within the coating layer under different loading conditions, which is necessary for improving the load-carrying capability of the coating. Unlike previous studies, the multilayer diamond-like carbon (DLC) coatings having high elastic modulus and hardness were analysed in this work. Under normal contact conditions, plastic deformation occurs in contacting materials when the contact pressure is greater than the hardness of the materials. Therefore, high hardness coatings can resist plastic deformation to avoid failure of the coating; in addition, multilayer coatings can decrease stress concentration to avoid cracking.

The purpose of this study is to determine whether DLC multilayer coatings can improve the property of the coating against potential cracking in the coating. It has been shown that structurally graded coatings had effect on reducing the contact-induced stress among all the factors considered. It is anticipated that the multilayer design parameters will be important to understand the stress distribution within metal-on-metal (MOM) hip replacements.

DECLARATION

I certify that this thesis does not, to the best my knowledge and belief:

I. incorporate without acknowledgement any material previously submitted for a degree or diploma in any institution of higher education;
II. contain any material previously published or written by another person except where due reference is made in the text; or
III. contain any defamatory material.

I also grant permission for the Library at the Edith Cowan University to make duplicate copies of my thesis as required.

ACKNOWLEDGEMENS

It is my great pleasure to thank my supervisor ***Dr Zonghan Xie,*** and associate supervisor ***Dr Xiaoli Zhao*** who steered me in the right direction, guided and supported me throughout this research period. Without their kind assistance and encouragement, this study would have never been accomplished.

I would like to express my deepest gratitude to all my family members and friends for their moral support, so I can comfort in the study at ECU, Perth.

Finally, infinite thankfulness is given to my girlfriend for her understanding and support.

NOTATION

Basic SI units are given in parentheses.

d	distance along the interface between the coating to subtract (μm)
D_H	diameter of the head (mm)
D_C	diameter of cup (mm)
h	indentation depth of the coating (μm)
H_c	clearance between the head and cup (mm)
N	normal force acting on the failure plane (N)
δ	thickness of the cup (mm)
σ_r	normal radial stress (GPa)
τ_r	shear stress of the DLC coating (GPa)

LIST OF TABLES

LIST OF FIGURES

CONTENTS

CHAPTER 1

INTRODUCTION

1.1 General background

The hip joint is the biggest joint in the human body; it is composed of two parts: the socket (acetabulum) from the pelvis, and the ball, from the femur (Igli, 2002). It is reported that about 3% of all adults over the age of 30 in America have joint diseases that often lead to the need for hip joint replacement (Felson et al., 2000). A hip joint replacement is a surgical procedure; that is, the bone of the hip joint is replaced with artificial materials.

Many studies of some early designs have shown that some total hip joint replacements can last 20 or 30 years (Streicher et al., 1996; Semlitsch and Willert, 1997); however, other studies of some early designs have shown that dramatic short-term failure can happen within 2 years (Walker and Gold, 1971). The benefits of hip joint replacement have been discussed in previous studies (Wagner, 1978; McMinn et al., 1996; Wagner, 1996; Amstutz, et al., 1998), wherein many hip joint replacement designs were tried and reported on. The early results of the hip joint replacement procedure were simple, and most of the concepts was abandoned (Schmalzried et al., 1996).

Metal-on-metal hip replacement is an artificial hip joint where both the cup and head are metal. Cobalt-chromium-molybdenum (CoCrMo) was an excellent material for the substrate of hip joint replacement. Jakobsen et al. (2010) found CoCrMo porous bead-coated implants decrease about 40% of biomechanical fixation contrast to titanium porous bead-coated hip joint replacement. Poliakov et al. (2004) reported that the alloy is a better material to use for artificial hip joint than Ti and stainless

steel, based on experimental and literature data. However, there are some drawbacks: CoCrMo might become corroded and show wear and release of metal ions once it is exposed to a disadvantageous environment (Shah et al., 1999; Huang et al., 2003). DLC coatings can effectively reduce the volumetric wear of metal-on-metal hip joint implants by protecting the polished surfaces of the hip joint replacement from damage. The maximum Young's modulus of diamond like carbon DLC coating on Co–Cr–Mo alloy attains 500 GPa (Poliakov et al., 2004). High hardness coating can resist plastic deformation to avoid coating failure; in addition, multilayer coatings can decrease the stress concentration and avoid crack. For this reason, high elastic modular and hardness of DLC multilayer coatings can improve the property of the coating..

1.2 The reason for hip joint replacement failure

Failure of hip joint replacement is mainly due to damage to the head, caused by the wear particles separating from the DLC coating. The failure appeared as a result of high contact stress at the surface of the coating. In addition, the contact stresses were associated with contact areas between the head and the liner.

The process of layer delamination from the interface of the coating with the substrate is a result of layer stress; stress increases when the contact area is reduced. Besides, the stresses might vary rapidly as some large particles appear on the contact surface between the head and the cup. Under the same loading, stress would increase when the contact area reduces, which will happen in the vicinity of wearing debris. As such, once wear debris is generated, a catastrophic process could be initiated, resulting in more stress/corrosion/cracking. As such, acquiring a strong coating without failure is highly desirable for the applications of hip joint replacement. Fig 1.1 shows the picture of the crack and delamination of the coating. According to the previous studies, the process can be considered as a stress-corrosion-cracking mechanism (Falub, Thorwarth et al. 2009). Thus, acquiring coating that will not fail is very important for the surface of hip joint replacement, and it is necessary to research the stress behaviour of the coating and improve the property of the coating by varying the structure of the coating.

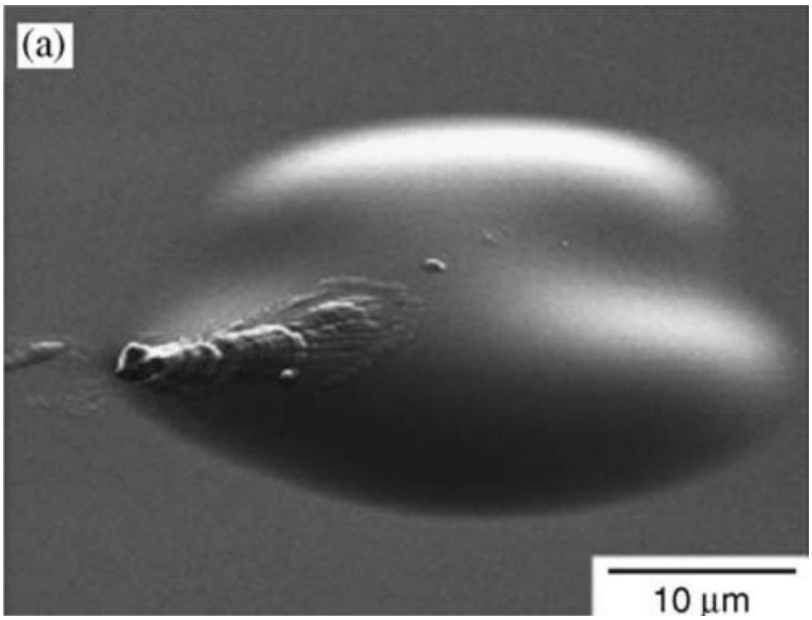

(a)

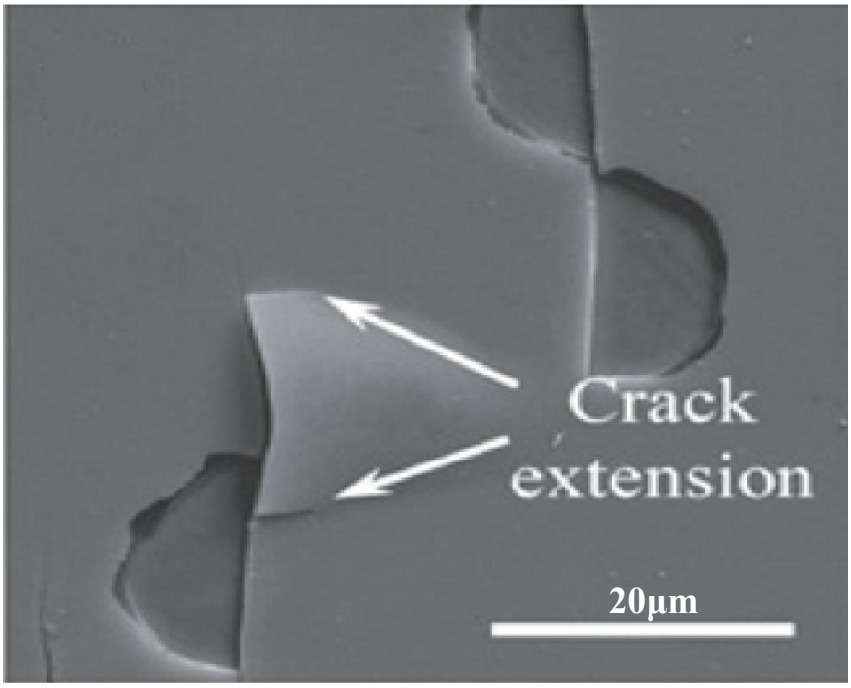

(b)

Fig 1.1. Examples of buckle delaminations and crack on the DLC coating: (a) buckle delaminations (Faulhaber et al., 2006); (b) crack extension observed in a thin DLC coating (Kim et al., 2007).

1.3 Objectives and scope of the present work

In the available literature, various methods have been used to decrease the failure of hip joint replacement. In recent years, diamond-like carbon DLC has appeared as an excellent coating material, due to its high wear and corrosion

resistance, high hardness, and low frictional coefficient. All these merits prove DLC as a good material for hip joint replacement. DLC coatings can be easily alloyed and doped with other different materials because of its amorphous structure. This brings on a broad range of merits, relying on its sp3, sp2, and hydrogen content when combined with the elements incorporated. One limitation is that low hardness and young's modular DLC coating were adopted in previous research studies. There is no high hardness coating, and high Young's modulus DLC coating is dependent on the substrate. Under normal contact conditions, plastic deformation appears in contacting materials when the contact pressure is greater than the hardness of the materials (Singh et al., 2010). Therefore, high hardness material can protect the coating from damage caused by plastic deformation. Stress concentration might be in the interface between the coating and substrate if only one DLC coating is deposited on the substrate. In order to decrease the stress concentration, three different structures of coating were designed in this work: one-layer coating, three-layer coating, and five-layer coating. All three coating systems have the same thickness—4 μm. Note that a similar coating thickness is frequently used in the real application of artificial joints.

For the diameter of the head, Reed (2000) has compared four different sizes of hip joint replacement heads. His results suggest that a femoral head of 28 mm in diameter can increase the range of motion after total hip replacement. Cosmi et al. (2006) designed two different metal-on-metal total hip joint replacements to compare the conditions of wear, and they reported that the larger hip joint replacement head (50 mm) produced more wear volume than the smaller one (28 mm). Therefore, in our work, a diameter of 28 mm was adapted for the FEM model.

In this study, the finite element analysis software COMSOL Multiphysics 3.5a was used to map stress distributions within DLC-based multilayer coatings on CoCrMo alloys, under loadings during normal applications. Coatings with different numbers of layers were modelled and compared; the results of this study can help improve our understanding of coating structures and help design and optimize the surface integrity of coated artificial joints.

This work aims to study the DLC coating stress distribution by changing the structure of the coating. Major objectives of this study are:

- Creating the three different types of layers of the DLC multilayers coating modelling with different Young's modulus in each layer.
- Analysing the normal distribution structure (one-layer coating) of the DLC coating on the hip joint replacement.
- Analysing the distribution of three-layer coating and five-layer coating which are presented in this study.
- Comparing the result between normal structure coating and multiple layer coating.
- Studying the link between stress distribution and cracks that can occur in the DLC coating.

1.4 Organisation of thesis

The general details of the thesis are described in this chapter. Chapter 2 presents a critical review of the literature on the analyses of the hip joint replacement, their causes, and the failure of the hip joint replacement. The characteristics of coating and the reasons for cracking and delamination also were researched. Both the experiment and finite element modelling (FEM) methods have been applied for analyses of the hip joint replacement and have mapped the distribution of the stress in the contact surface. The review establishes the need for this research and the appropriateness of methods chosen. The configuration and preparation of the three different types of layer coating modelling are described in Chapter 3. The result of the stress distribution and deformation are presented in Chapter 4. The normal stresses and shear stresses are discussed in Chapter 5, to help research the link between cracks and stresses. The summary and general conclusions, along with future recommendations, are presented in Chapter 6.

CHAPTER 2
LITERATURE REVIEW

2.1 General

A hard coating layer on the surface of the ball in artificial hip joint replacements is important for enhancing the lifespan of these biomedical implant components. Diamond-like carbon (DLC) is an excellent coating material for a variety of industrial and other applications. Recently, it has been applied as a coating material on artificial hip joints, with considerable success (Nir 1987; Deng and Braun 1995; Cui and Li 2000; Tilbrook et al., 2007). However, results were also reported that there were material defects within the DLC coatings, which resulted in increased wear and coating delamination (Schwarz et al., 2008). Ward suggested that the failure of hip joint replacement may well be correlated with the wear particles (Ward et al., 2010). Tipper et al. (Tipper et al., 2000) analysed the wear particles, wear rate, and damage of the head surface in hip joint replacement. Their results indicated that high femoral head damage was correlated with increased total wear volume.

Delamination or failure within the coating of artificial joints occur when stress reaches a critical level, resulting in large wear debris particles (Fig 2.1) appearing on the contact surface between the head and the cup. The process has been described as being due to a stress-cracking mechanism (Falub et al., 2009). Under the same loading, stress increases when the contact area reduces, which will happen in the vicinity of wearing debris. As such, once wear debris is generated, a catastrophic process could be initiated, resulting in more stress-cracking. As such, acquiring a strong coating without failure was highly desirable for the applications of hip joint replacement. Failure in a coating layer is normally initiated by excessive local tensile or shear stress; therefore, it is important to clarify the stress distribution within the

coating layer under different loading conditions, which is necessary for improving the loading carrying capability of the coating.

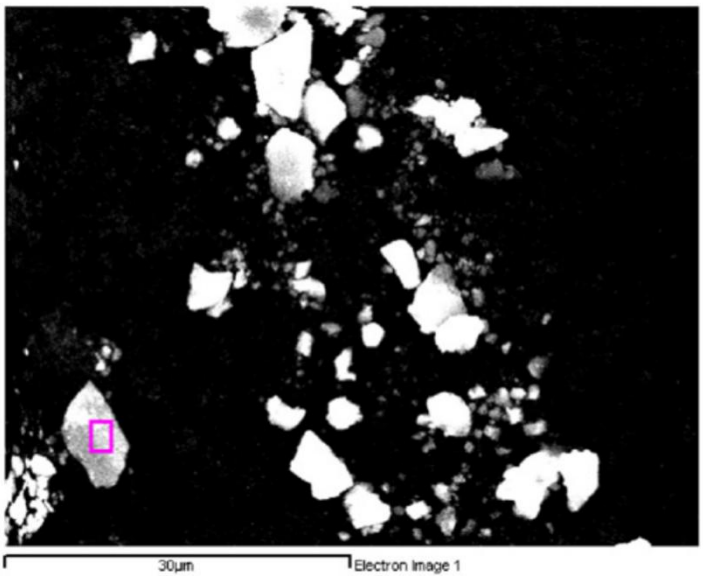

Fig 2.1 A picture of DLC particles resulted from wear in artificial hip joint (Wong et al., 2010).

The size of the head was an important parameter for determining the overall performance of artificial hip joints. Reed et al. (2000) compared four different sizes of hip joint replacement head. Their results suggest that a femoral head 28 mm in diameter can increase range of motion after total hip replacement. Compared with the 28 mm size head, the 22 mm size head always appeared to have dislocation secondary to prosthetic impingement.

Harris (1994) gave a review on particle disease and the influence of particles in hip joint replacement. That paper suggested that, considering particulate debris, the use of titanium femoral heads and 32 mm diameter femoral heads should be avoided. Cosmi et al. (2006) designed two different metal-on-metal (MOM) total hip joint replacements to compare wear conditions. They reported that the larger hip joint replacement head (50 mm) produced more wear volume than the smaller one (28 mm).

2.2 The properties of the materials

2.2.1 The material of the CoCrMo substrate

CoCrMo is an excellent material for the substrate of hip joint replacement. Jakobsen (2010) found CoCrMo porous bead-coated implants decrease about 40% of biomechanical fixation, in contrast to titanium porous bead-coated hip joint replacement.

Poliakov et al. (2004) reported that CoCrMo alloy is a better material to use for artificial hip joint than Ti and stainless steel, based on experimental and literature data.

2.2.2 The material of the DLC coating

Cui and Li (2000) reviewed the mechanical properties of diamond-like carbon (DLC), particularly its excellent adhesion, as well as its unusual desirable properties. It has a wide range of applications in biomedical engineering.

Thorwarth et al. (2010) investigated the tribological behaviour of DLC coatings in hip joint replacement. Their results showed that good interfaces will avoid delaminating under high load during extended periods of testing. In addition, DLC coatings can effectively reduce the volumetric wear of metal-on-metal hip joint implants by protecting the polished surfaces of the hip joint replacement from damage.

There are also a number of metals that have been used as the material of biomedical applications—for example, titanium and cobalt–chromium alloy (Shah et al. 1999; Huang et al., 2003). However, these common materials might become corroded, produce wear, and release metal ions once they are subjected to a disadvantageous environment. For example, stainless steel can corrode, although it has been used in different biomedical applications with reasonable success.

Metal ions and other particles released from hip joint replacement are a possible cause of allergic reactions, and they can even cause tumours, as in the case of Ni (Gillespie et al. 1988); as such, there is growing interest in searching for inert and less degradable biomaterials for their wide use in clinical applications.

In recent years, diamond-like carbon (DLC) has appeared as an excellent coating material due to its high wear and corrosion resistance, high hardness, and low friction coefficient. All these merits have proven DLC as a good material for hip joint replacement. DLC coatings can be easily alloyed and doped with other different materials because of its amorphous structure. This brings on a broad range of merits relying on its sp^3, sp^2, and hydrogen content when combining with the element incorporated.

Wong et al. (2010) found that the hardness of DLCs is associated with the content of their sp^3 and sp^2 carbon structures. A new method has been proposed for obtaining the hardness of very tiny worn DLC particles dependent on their micro-Raman spectrum signals. The author has presented a new method to obtain the hardness of the diamond-like carbon debris.

During the wear process, worn material is delaminated from the contact surfaces in the form of particles. Cui and Li (2000) reported that wear that the generation of wear particles because of friction can lead to severe adverse reactions of the body.

Tipper et al. (1999) studied wear particles from CoCr alloys which had been used in MOM implants. Quantitative results of nanometer-sized wear debris from in vitro wear tests, and the influence of volume of wear and carbon content in MOM implants, were reported.

2.3 Experiment and finite element modelling (FEM)

A number of experimental and FEM analyses of stress distributions, deformation, and friction in hip joint replacement also have been investigated in previous studies.

2.3.1 Experiment

Wang, Essner, and Klein (2001) proposed an experimental method for analysis of the friction and wear in hip joint replacement (Fig 2.2). In their study, semicrystalline polymers in dry sliding were similar to the wear debris, which allows the simulation of the dependence of the coefficient of friction on contact stress. It was reported that the friction measurements were highly correlated with the wear rates measured on similar components.

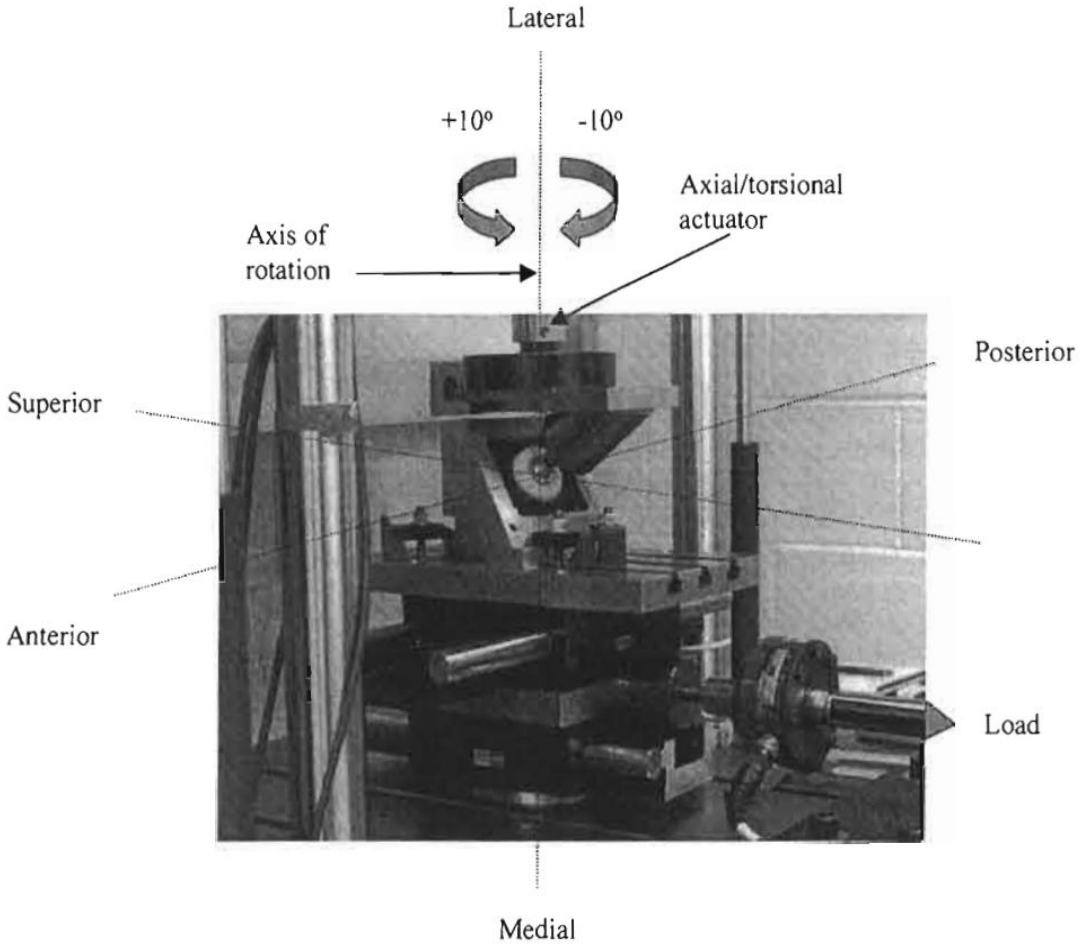

Fig. 2.2 Picture of the experimental method for analysis of friction and wear in hip joint replacement (Wang et al. 2001)

2.3.2 FEM method

Anderson et al. (2008) adopted the FEM methods to analyse contact stresses and load distribution in the pathologic and normal joint. They presented the approaches for using FEM modelling of hip joint in obtaining contact pressures and areas (Fig 2.3).

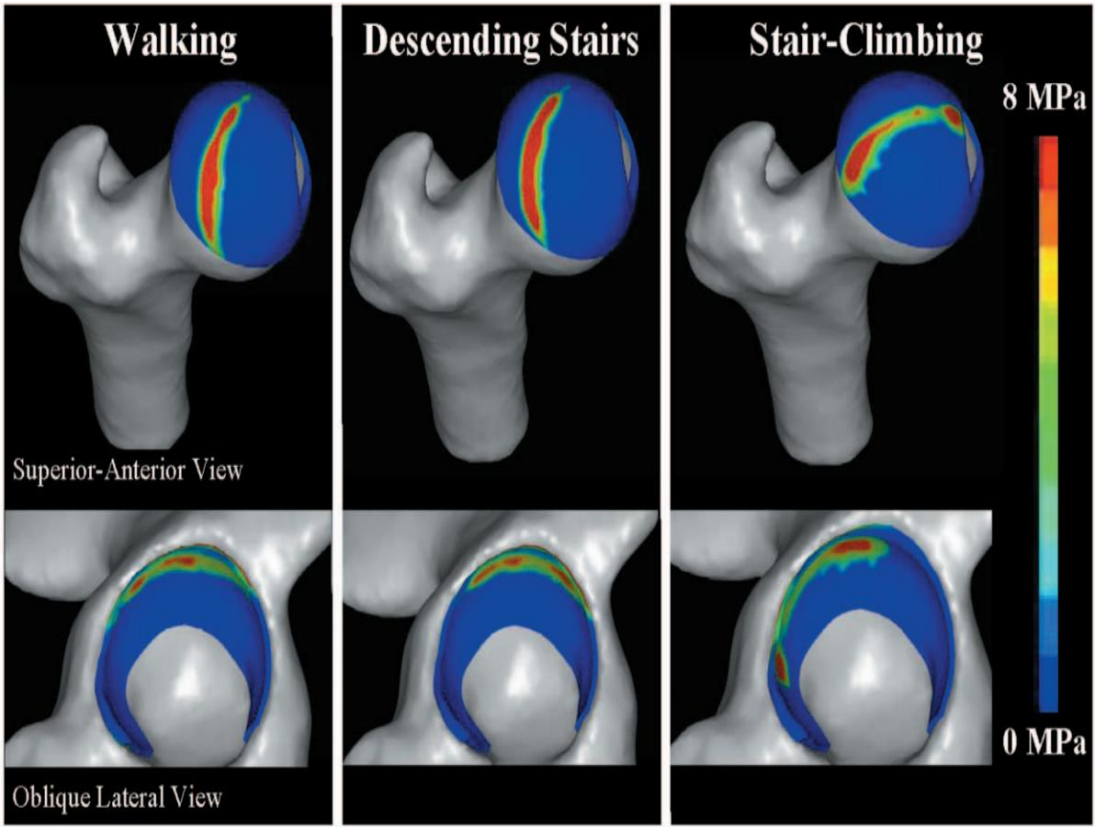

Fig. 2.3 FEM-predicted contact pressures on the femur and acetabulum with different actions (Anderson et al., 2008)

Investigation through the FEM method is a popular modal-based approach, which has been widely adopted in the published literature. A report on a two-dimensional model has been presented (Rapperport et al. 1985) (Fig 2.4), and it was concluded that pressure distributions, contact areas, and bone stresses obtained from the FEM model were different from those from the anatomic model and deformable pubic symphysis model.

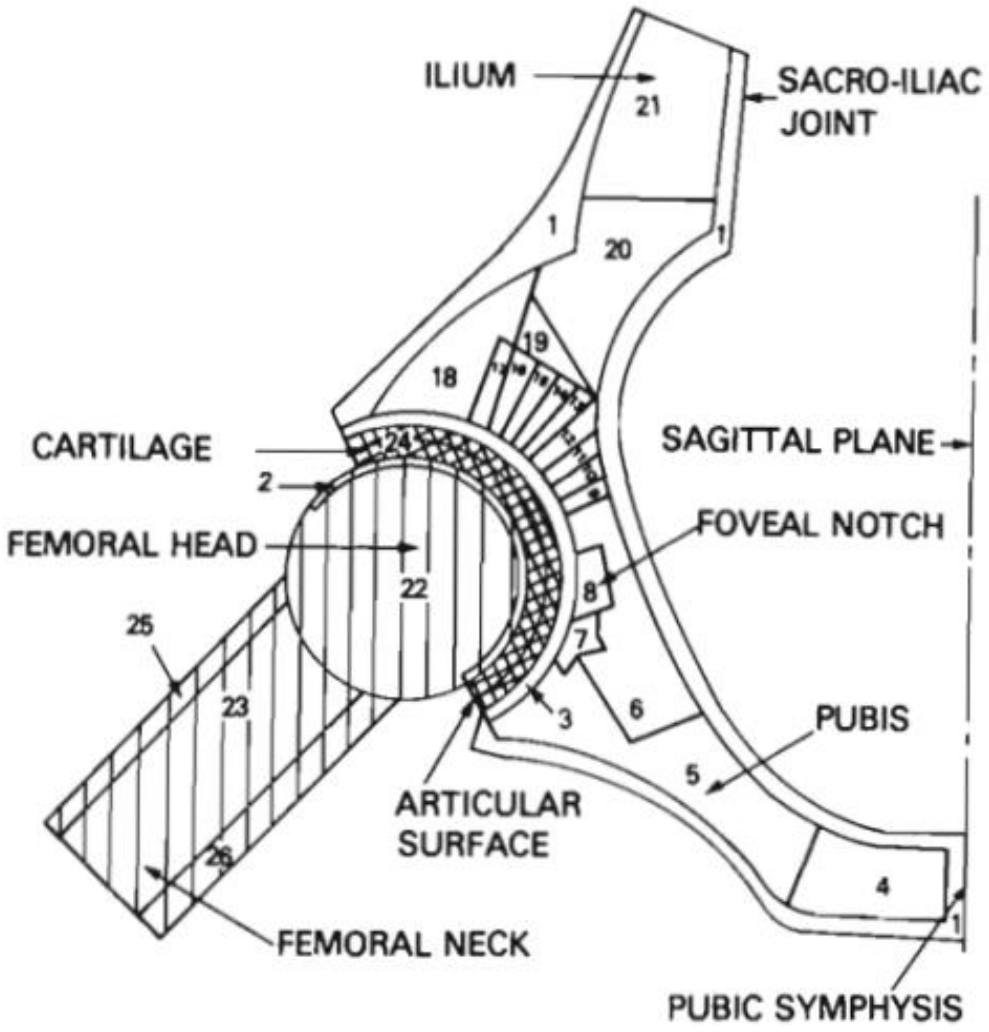

Fig. 2.4 Two-dimensional model (Rapperport et al., 1985)

Cilingir (2010) studied ceramic-on-ceramic hip replacement, using the FEM analysis method (Fig 2.5). The resulting distribution of von Mises stresses is shown in Fig 2.6. This work analysed the effects of radial clearance and loading and bone quality, and compared the results of coating on the implants and alumina.

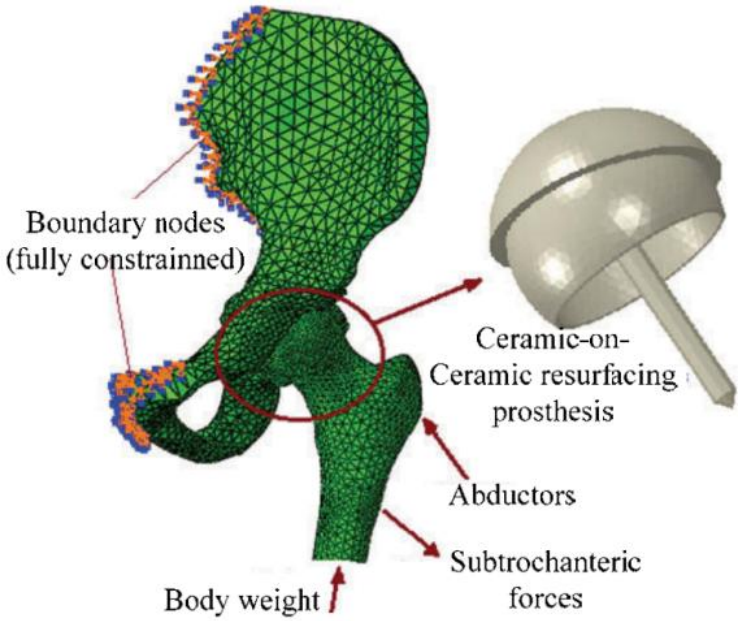

Fig. 2.5 3D FEM model of ceramic-on-ceramic hip joint replacement (Cilingir, 2010).

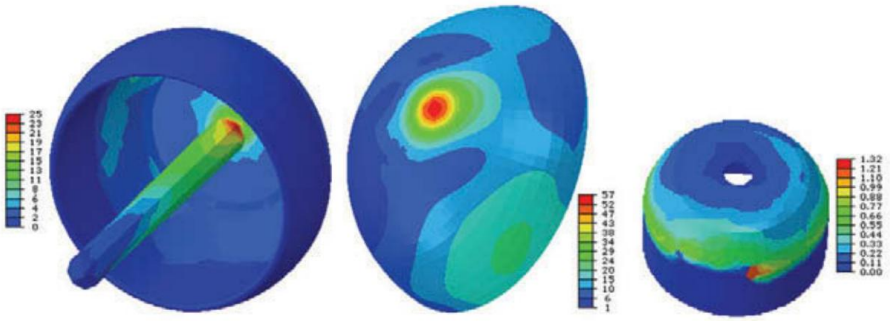

Fig. 2.6 The distribution of von Mises stresses (Cilingir, 2010).

Investigation using the boundary element method (Fig. 2.7) is another popular modal-based approach, which also has been widely adopted in the published literature. Sfantos and Aliabadi (2007) applied a model-based approach to analyse total hip joint replacement wear using a boundary element method. The results obtained were in good agreement with those from other researchers.

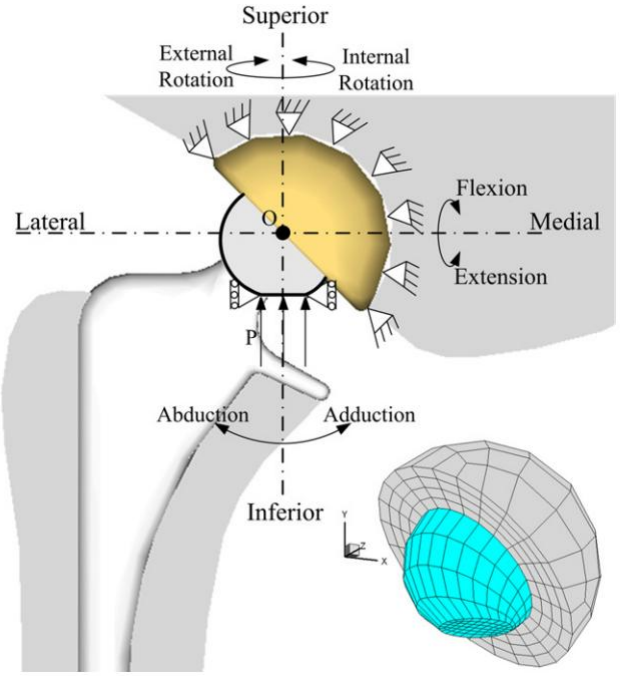

Fig. 2.7 Picture of the FEM model (Sfantos and Aliabadi, 2007).

Liu et al. (2010) focused on the coupling of dynamics and contact mechanics of hip joints replacement in a pendulum model (Fig2.8). In their work, an approach was developed for predicting the potential interaction between contact mechanics and dynamics for THRsusing both decoupled and coupled methods.

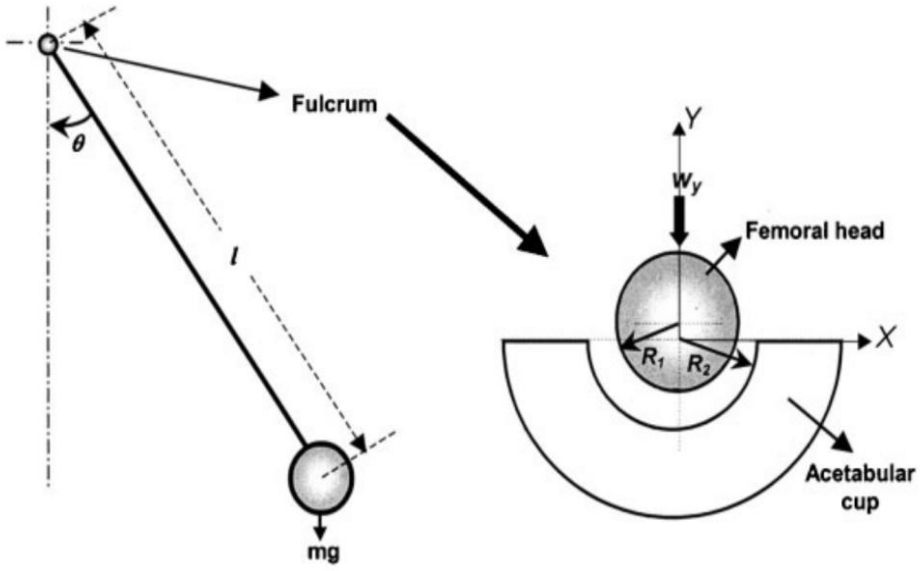

Fig. 2.8 Picture of the pendulum model (Liu et al. 2010).

Kang et al. (2009) reported on the relationship between wear and head size. The result of increasing the size of the femoral head was shown to increase the amount of wear debris, which was due to reduced contact pressure and increased sliding distance.

Bachtar et al. (2006) presented a new method that can be used for smoothing of discretised contact surfaces with Gregory patches, to avoid computation instability . The results of stress distribution in the hip joint head while standing were thus obtained (Fig 2.9).

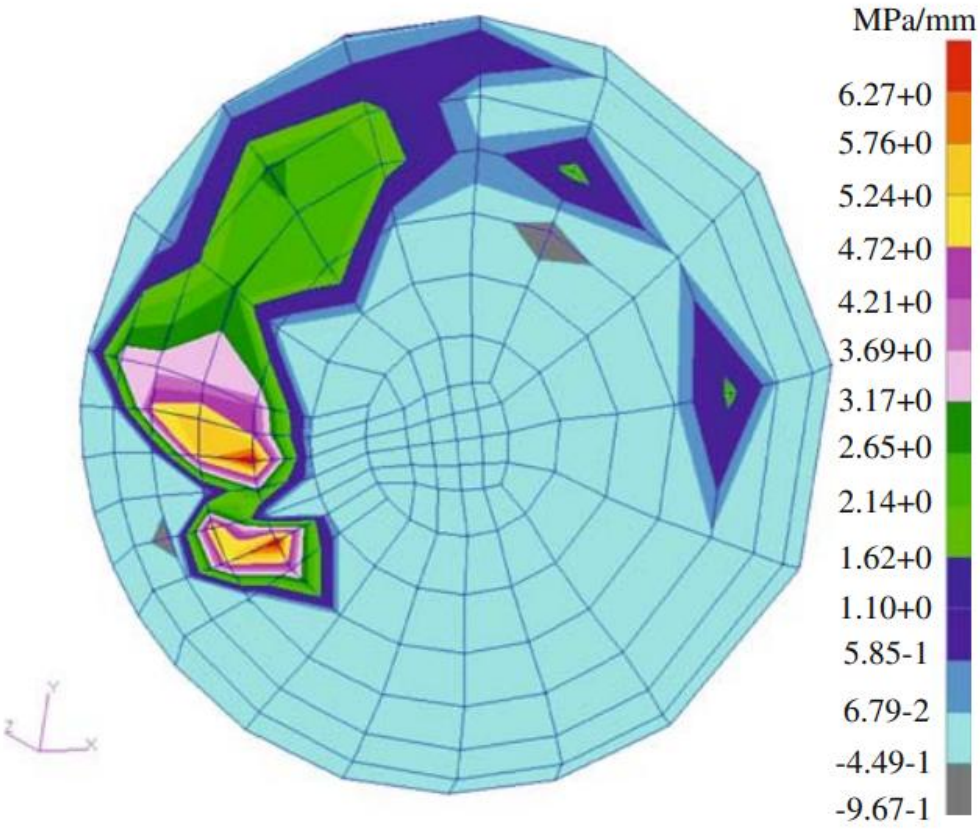

Fig. 2.9 Stress distribution in the hip joint head (Bachtar et al. 2006).

Kluess et al. (2007) studied the influence of hip joint head size on impingement, wear, and stress distribution in hip joint replacement. They reported that the femoral head with a diameter of 40 mm resulted in higher amounts of wear than the one with

a diameter of 28 mm. The stresses decrease when the diameter of the femoral head is larger.

Singh et al. (2010) presented a new approach to meliorate the toughness of DLC coating. They created three different coating systems. The first system was produced by gradually varying elastic modulus (E) from the top surface (higher E) to the interface (lower E). The second system has an opposite gradient in elastic modulus from the surface (lower E) to the interface (higher E). The last system is a unique one with the highest elastic modulus (E) value placed at the mid-plane of the carbon coating thickness. The third system has a better performance in protection the system from contact damage at both the surface and the interface.

Cruz et al. (2006) manufactured DLC multilayer coatings to study the properties. They report that the properties of the multilayer coatings were affected by the DLC structure, and that the hardness of the system, when using multilayer coating, changed from 21.7 GPa to 27.8 GPa.

Deng et al. (1995) presented a new method to analyse Ti/TiN/TiCN/TiC/DLC compositionally graded coatings (Fig 2.10). This paper has shown excellent mechanical and tribological properties.

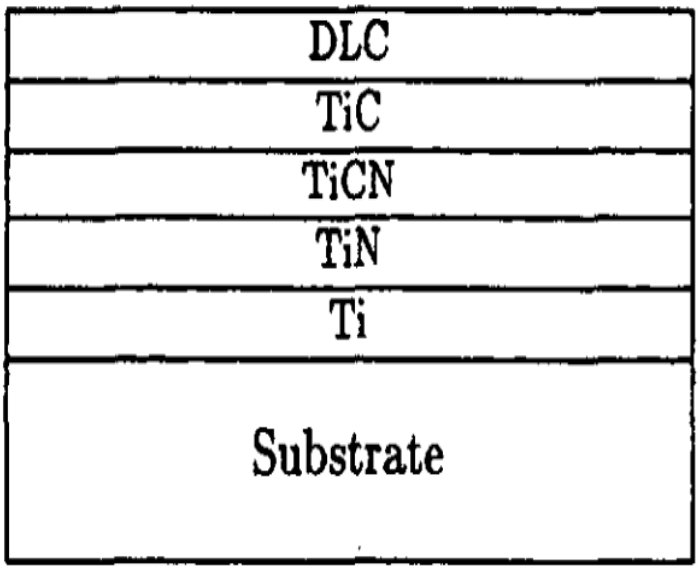

Fig.2.10 The structure of DLC compositionally graded coatings (Deng and Braun, 1995)

Zhang et al. (2006) presented multilayer coating systems (Fig 2.11) with graded properties to analyse the thermal residual stresses distribution. In their paper, the effects of the elastic modulus and other properties of the substrate and the coating layer (ZrO_2/NiCoCrAlY) were discussed. They reported that the total strain of the coating or the substrate was divided into a bending strain and a stress strain in this graded system.

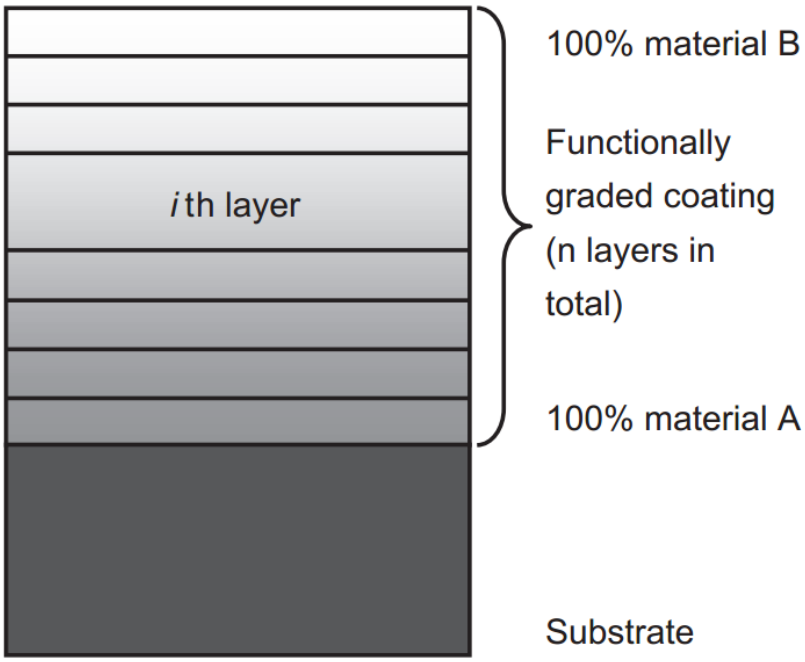

Fig. 2.11 The structure of the graded coating system (Zhang et al. 2006).

Bentzon et al. (1995) presented an experimental method to obtain the interfacial shear strength of the DLC coating. They reported that "the interfacial shear strength obtained between diamond-like carbon and steel is of the same order as the strength of the steel".

Zhao et al. (2011) analysed TiSiN-based multilayer coatings stress distributions using FEM modelling (Fig 2.12). It was reported that the maximum radial tensile stress reduces 50% at the interface by structural layering.

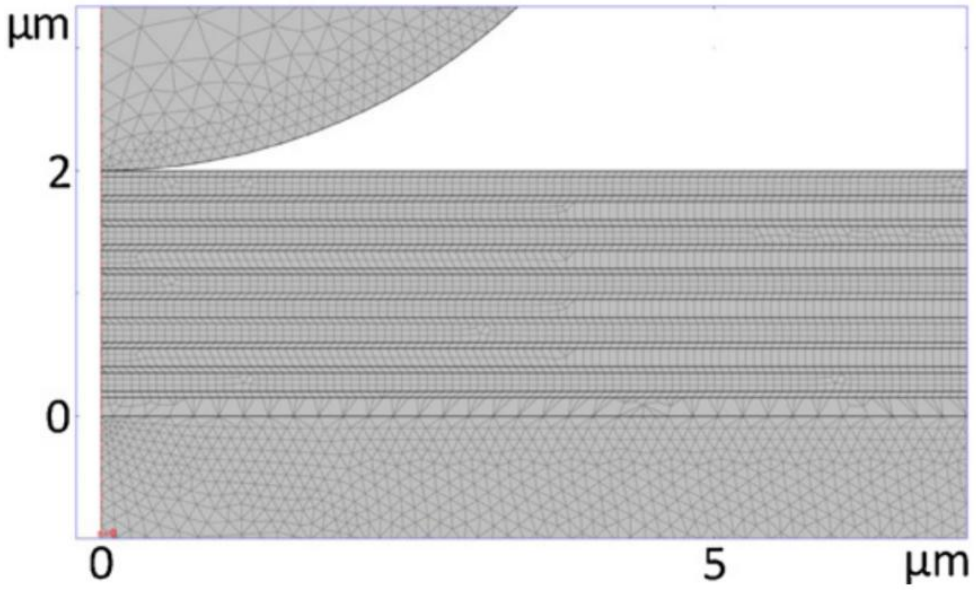

Fig. 2.12 The structure model of TiSiN-based multilayer coatings (Zhao et al., 2011).

Singh et al. (2008) observed the evolution of damage in the DLC coating system (Fig 2.13). They reported the likelihood of initiation of the ring and radial cracks under different loading conditions.

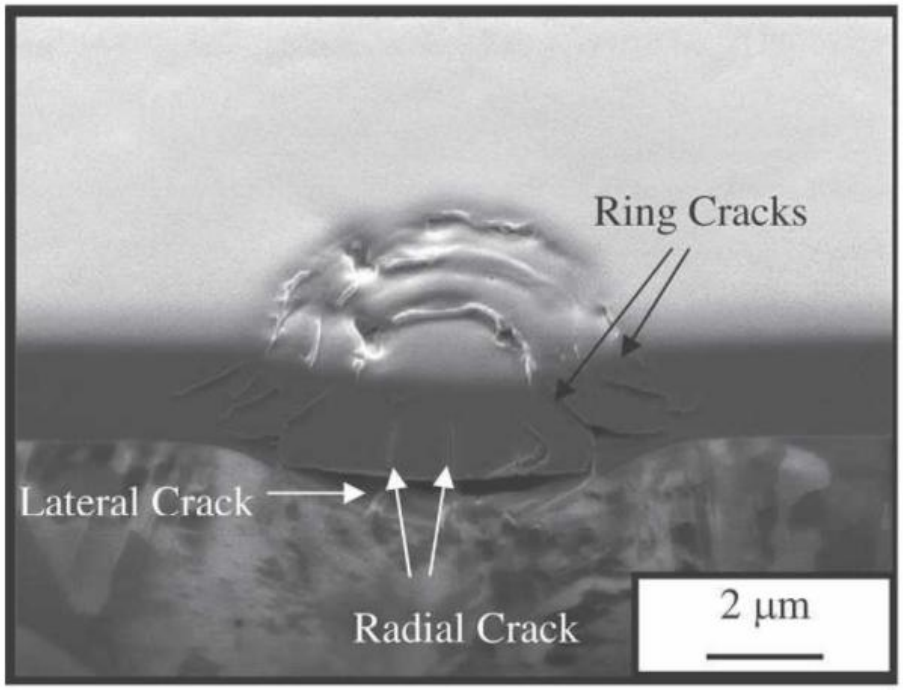

Fig. 2.13 Damage in the DLC coating system (Singh et al., 2008)

Unlike previous studies, DLC multilayer coatings with high hardness and elastic modulus were designed in this work. Under normal contact conditions, plastic deformation appears in contacting materials if the contact pressure is greater than the material's hardness (Singh et al., 2010). Therefore, a high hardness coating can resist plastic deformation to avoid the failure of coating; in addition, multilayer coatings can decrease stress concentration to avoid cracking.

CHAPTER 3
MODELLING AND DESIGN OF HIP JOINT REPLACEMENT

3.1 Introduction

The finite element method (FEM) is a numerical technique that is used to solve partial differential equations under specific boundary conditions, which are used to describe particular physical or engineering problems. Currently, FEM is employed in the simulation and modelling of different structures, including coating structures, in a wide range of applications.

There are three major phases in a typical FEM analysis process: pre-processing, analysis, and post-processing. The pre-processing phase includes procedures for preparing for the analysis phases, which includes the geometrical model of FEM, loading conditions, and application of the boundary conditions, as well as the properties of the material. The analysis phase, following the first step, is to analyse the finite element model developed. The analysis may be nonlinear or linear, dynamic or static, based on the nature of the FEM model being analysed, as well as the type of the results required. The purpose of the post-processing phase is to obtain the required results in their desired form. Frequently, the result is in the form of a colour-mapped image of stress distribution.

In this study, the finite element analysis software COMSOL Multiphysics 3.5a was employed.

3.2 Finite element model

A ball-and-socket model was presented to simulate the metal-on-metal hip joint replacement in this study; the radius of the head was 14 mm (Gao et al., 2009). The DLC layers were deposited on the surface of a CoCrMo biomedical implant alloy. The DLC coatings used in this study were approximately 4 μm thick (Falub et al.,

2011). Three different structures of DLC coating were modelled in this work: one-layer coating, three-layer coating, and five-layer coating. All three different kinds of coating have the same overall thickness — 4 μm thick. Note than a similar coating thickness is frequently used in the real application of artificial joints.

In this simulation, a 2D axial symmetry model was adopted to reduce computational time without compromising accuracy. It was assumed that the coating is perfectly adhered to the substrate and that all the interfaces between different layers were perfectly bonded. Static analysis was adopted. The effect of a microparticle or wear damage debris, sandwiched between the cup and the ball, was modelled as a vertical downward force that generates a spherical indentation on the top surface of the ball. Due to the fact that the ball is spherically symmetric, except for the base area, which is far away from the possible loading zones on a microscopic scale, this particular loading direction is only for modelling convenience and does not lose the generality. The whole structure of the hip joint replacement is shown in Fig. 3.1.

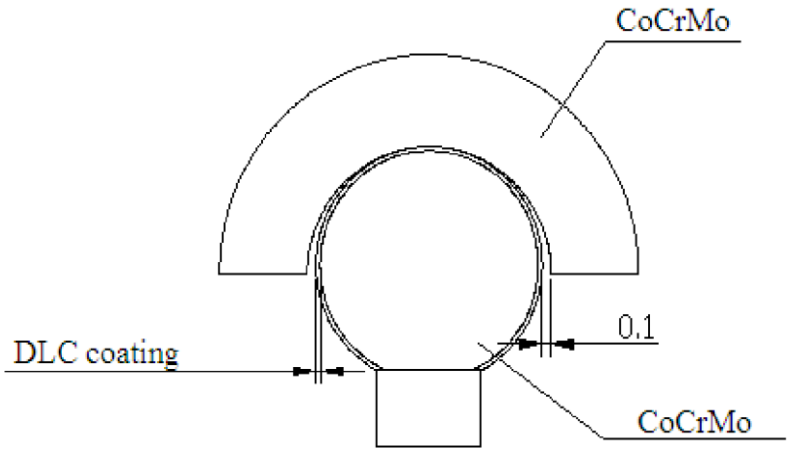

Fig. 3.1 Modelling of total hip joint replacement

Three different radius sizes (2.5 μm, 5 μm and 7.5 μm) of micro-particles were simulated, with the DLC coating and the CoCrMo substrate place at the right-hand side of the structure, as shown in Fig. 3.2. The bottom boundary and the left side boundary were fixed in the z and r directions, respectively. The rest of the boundaries were free to move. Free mesh was applied, and the mesh was refined within the region close to the loading and was further refined in the case of three- and five-layer coatings, as indicated in Fig. 3.2. The total number of degrees of freedom is 81,208,

and the number of elements is 19,730. The DLC coatings showed pure elastic deformation (Singh et al., 2008).

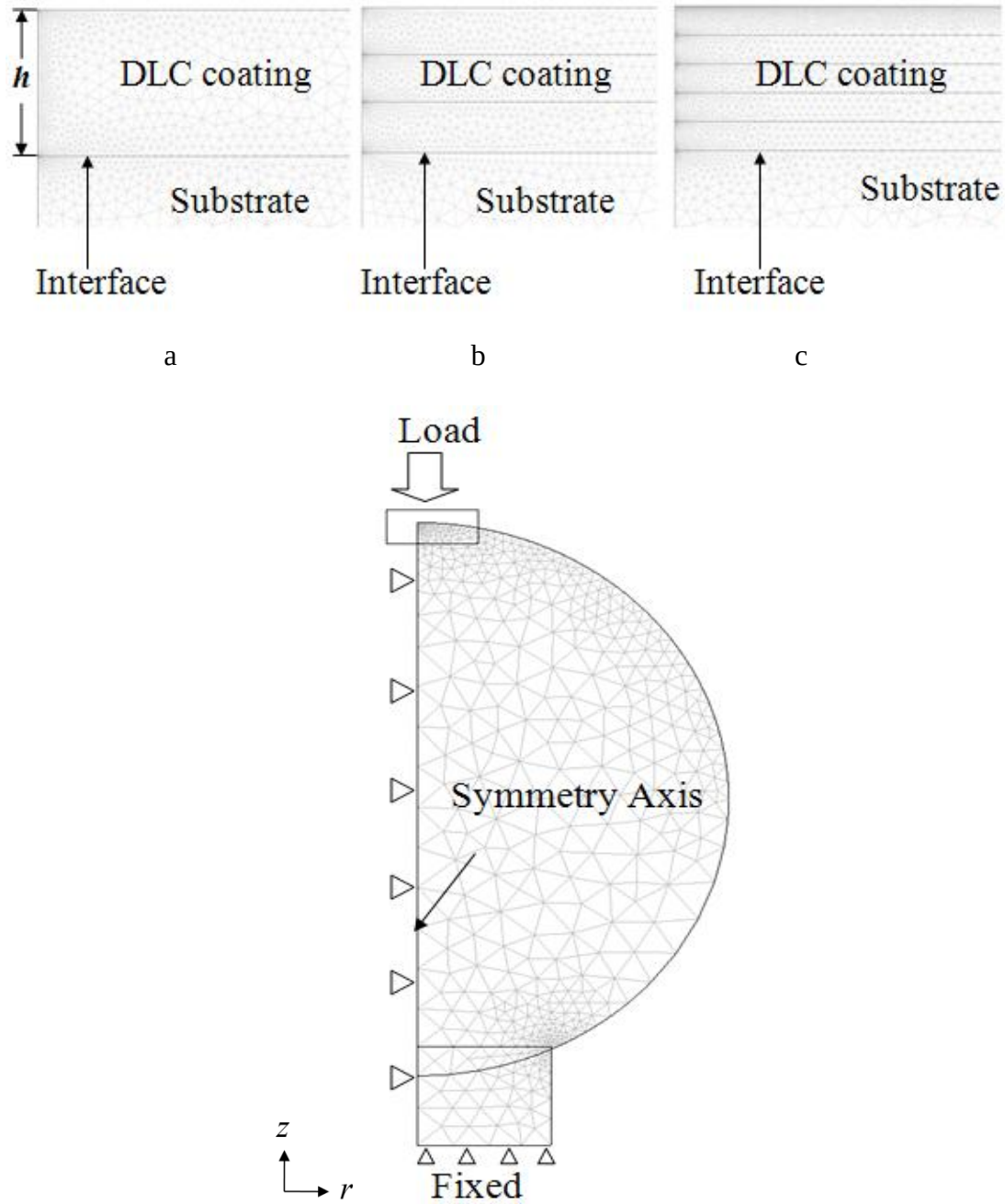

Fig. 3.2 Meshes used in the finite element models for (a) single-layer coating, (b) three-layer coating, and (c) five-layer coating on CoCrMo substrate

3.3 Parametric study

Table. 3.1 Parameters of FE model

Diameter of head D_H	Clearance H_C	Diameter of cup D_C	Thickness δ
28 mm	0.1 mm	28.1mm	10mm

For the head diameter , Reed et al. (2000) compared four different sizes of hip joint replacement head. Their results suggest that a femoral head of 28 mm in diameter can increase the range of motion after total hip replacement. Compared with 28 mm size head, 22 mm size head always appeared. Cosmi et al. (2006) designed two different metal-on-metal total hip joint replacements to compare the conditions of wear. They reported that the larger hip joint replacement head (50 mm) produced more wear volume than the smaller one (28 mm). Therefore, in our work a diameter of 28 mm was adopted for the FEM model.

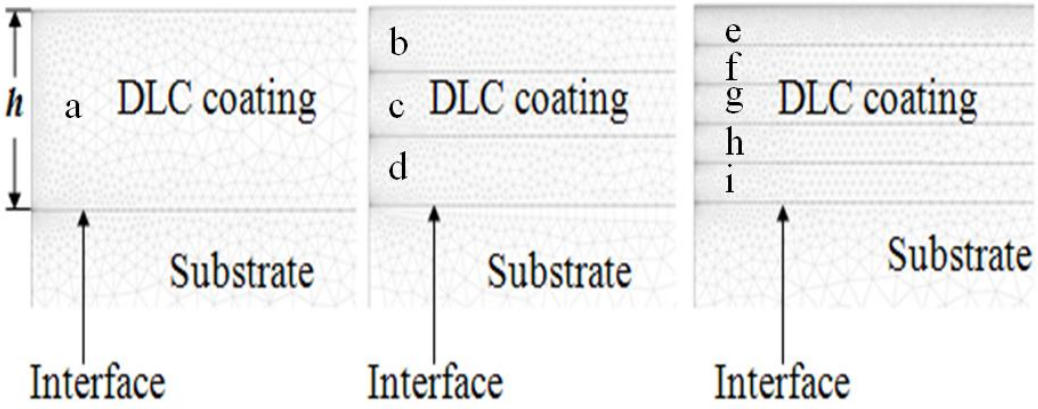

Fig.3.3 Structure of DLC coating

Table 3.2 The DLC Elastic modular with different layer

	1 layer	3 layers			5 layers				
Number of layers	a	b	c	d	e	f	g	h	i
DLC E modular (Gpa)	500	500	400	300	500	440	380	320	260

3.4 Material Properties

DLC coatings have been known to extend the operational lives of hip prostheses. It is an excellent coating material in a variety of industrial and other applications. Recently, it has been applied as a coating material on the artificial hip joint with considerable success.

A CoCrMo alloy is more suitable for artificial hip joint than Ti and stainless steel, based on experimental and literature data. Jakobsen (Jakobsen et al., 2010) found fixation of the CoCrMo porous bead-coated implants decrease a statistically significant 40%, compared with titanium porous bead-coated implants. In this work, CoCrMo is used consistently as the material of the substrate.

Young's modulus is a well-defined material property (Oliver and Pharr, 1992); the maximum Young's modulus of DLC films on CoCrMo alloy attains 500 GPa (Poliakov et al., 2004). Different Young's modulus (E) can be obtained by varying the bias voltage during processing. Thus, the Young's modulus (E) of the different layers was allowed to vary linearly, as listed in Table 3.2.

Table 3.3. The properties of materials involved in the modelling.

Parameters	E modulus(GPa)	Poisson's ratio	BH(GPa)
strength(GPa)			
DLC		0.33	
CoCrMo	200	0.3	1.7

The properties of materials were shown in Table3.3. E modulus of CoCrMo is 200 GPa and the Posson's ratio is 0.3. Bilinear kinematic hardening stress–strain curve is 1.7 GPa (Singh et al., 2008)

3.5 Loading

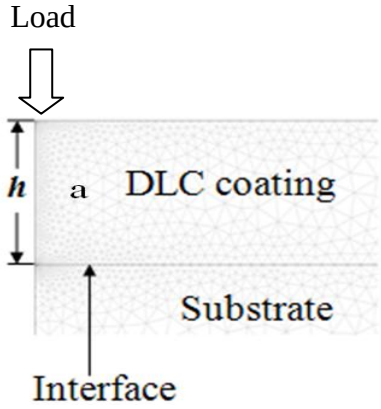

Fig.3.4 The position of load

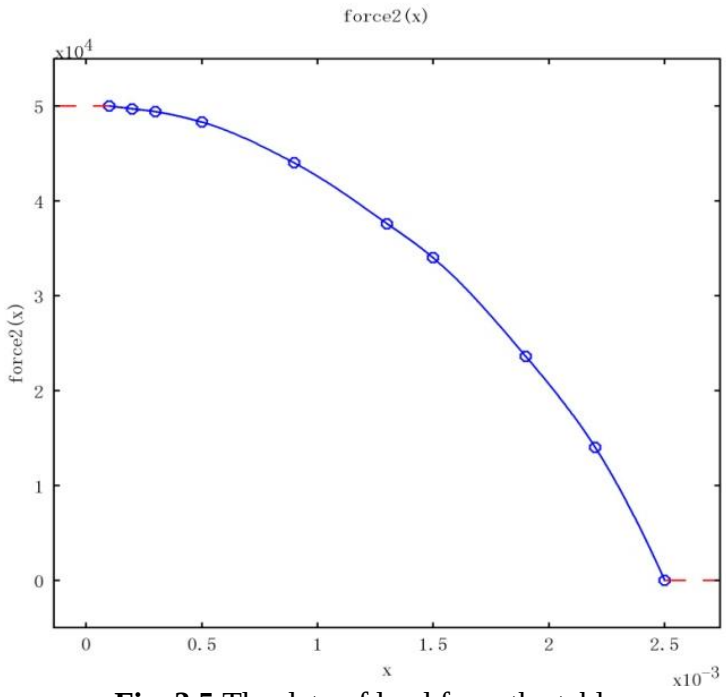

Fig. 3.5 The data of load from the table

The position of loading in the DLC coating is shown in Fig 3.4. The direction of the load is perpendicular and downward. The load decreased from the left-hand side to the right-hand of the model (Fig. 3.5). The loading was varied, so as to produce different indentation displacements on the hip joint replacement model.

CHAPTER 4
RESULTS

4.1 Introduction

The most important step of finite element analysis procedure is the physiologically realistic interpretation of the results by the analysis. Since finite element analysis procedures are invariably accompanied by an extensive output of data, it is extremely important that we interpret the results correctly.

In this chapter, the modelling results of radial stress and shear stress were presented. Three different types of DLC coatings were modelled in this work： one-layer coating, three-layer coating; and five-layer coating. All of the coatings have the same total thickness, with the sum of all the layers being 4 μm thick. The purpose of the modelling works is to evaluate the improvement that could be achieved using different multilayer coatings.

Three different indentation depths, due to different loading conditions, were modelled in the FEM coating model (Fig4.1). For the same displacement the stress distribution were compared between different coating structures. It is clear that three different indentation depths (*h*) were obtained in the top of the Fig .4.1, respectively, they were 0.25 μm, 0.5 μm and 0.75 μm.

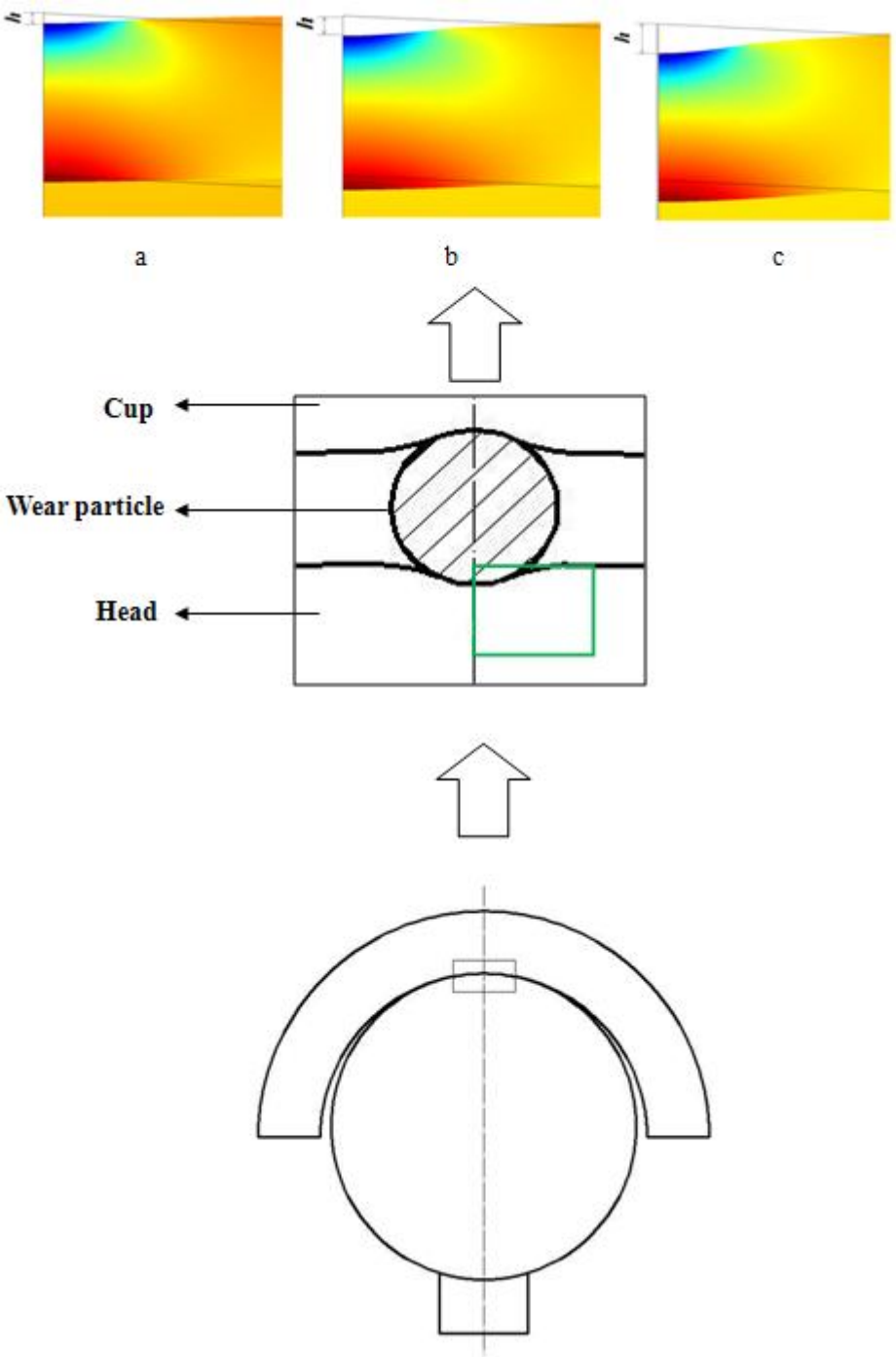

Fig.4.1 The displacement (*h*) of the model after different loadings: (a) displacement *h*=0.25 μm, (b) displacement *h*=0.5 μm, and (c) the displacement *h*=0.75 μm

4.2 Results and analysis

4.21 Radial stress

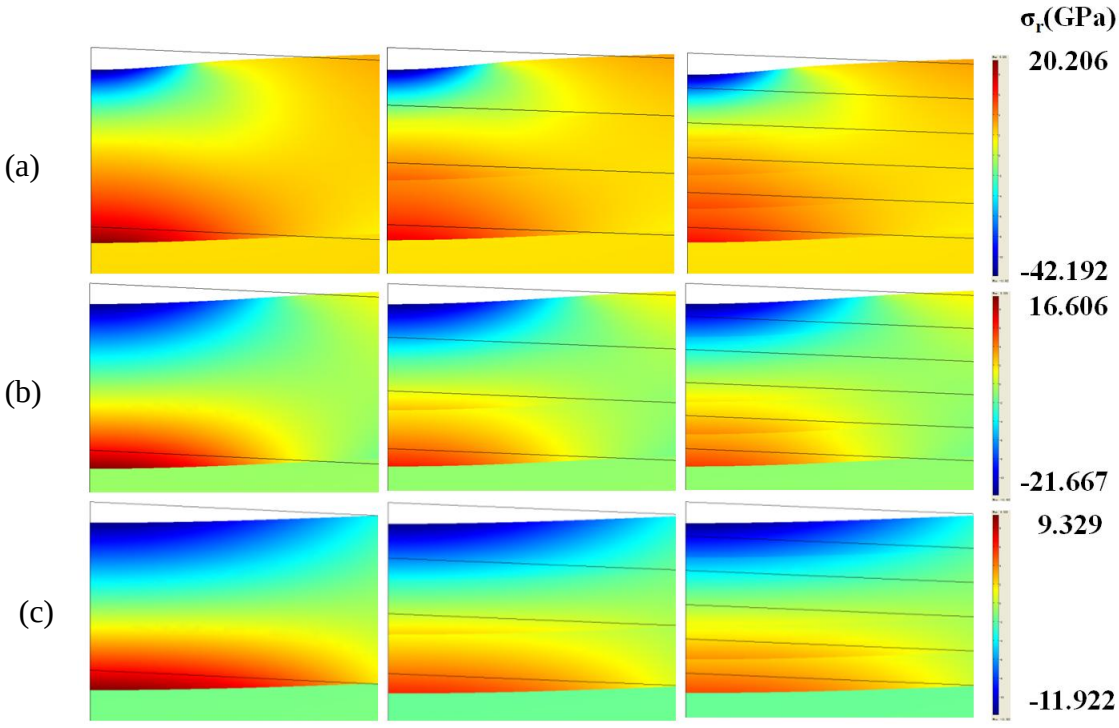

Fig.4.2 Distribution of radial stress (σ_r) at the indentation depth (h) of 0.5 μm, for wear particle of different radius, (a) 2.5 μm, (b) 5.0 μm, and (c) 10 μm.

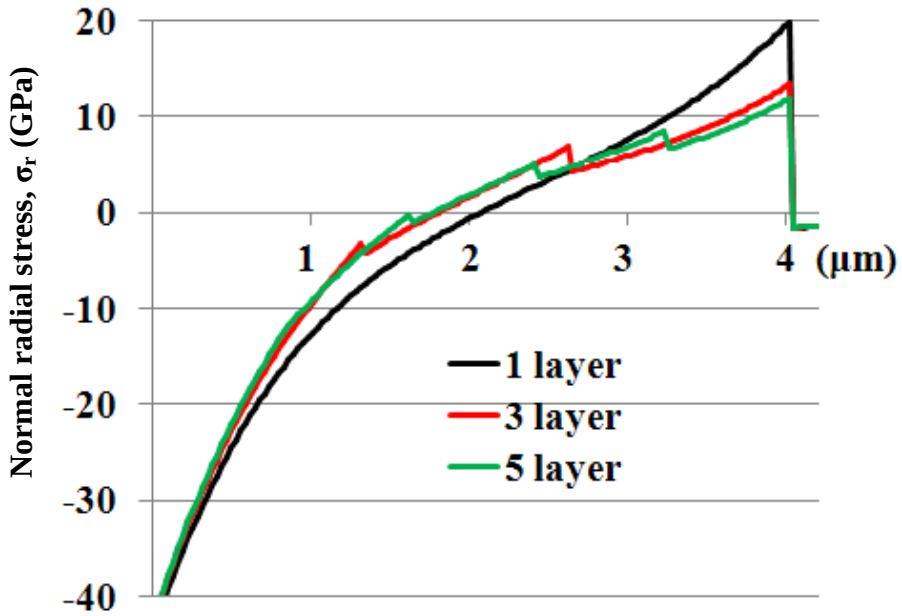

Distance, d (μm)

(a)

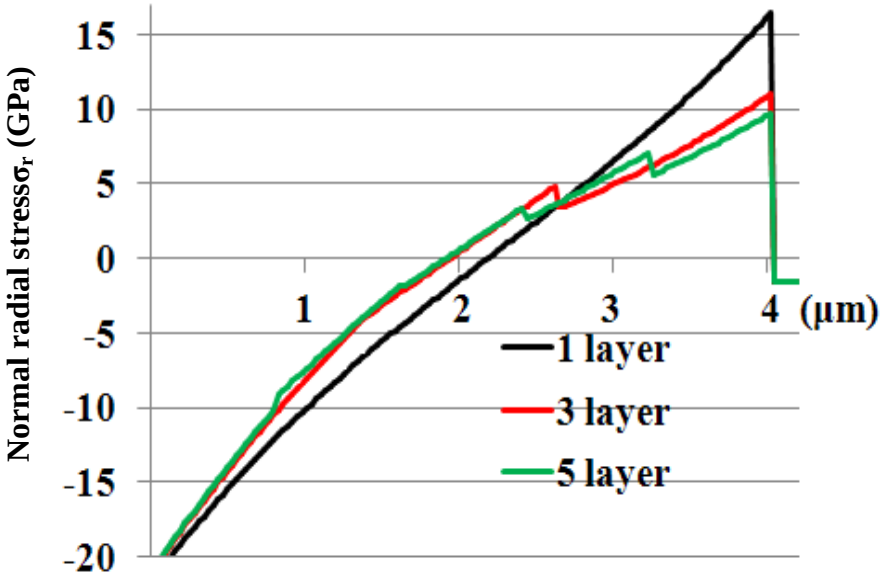

Distance, d (μm)

(b)

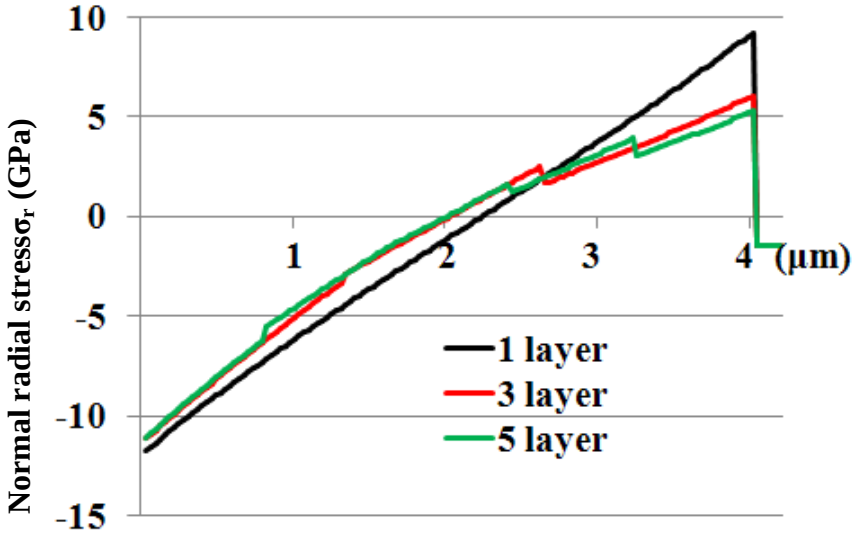

Distance, d(μm)

(c)

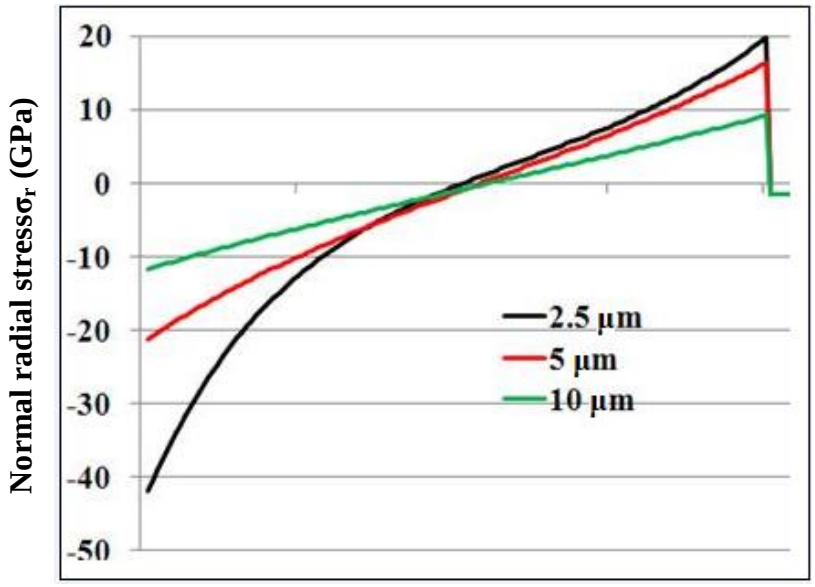

(d)

Fig. 4. 3 Normal radial stress distribution, $\boldsymbol{\sigma_r}$, along the symmetry axis, with one, three, and five layers of DLC coating, under the loading of the wear particle with a radius of (a) 2.5 µm, (b) 5 µm, and (c) 10 µm. (d) normal radial stress distribution of single-layer coating, σ_r, d is along the symmetry axis, in a monolithic coating under wear particles of different sizes.

The distributions of the normal radial stress loaded by three different particle sizes are shown in Fig. 4.2. It is clear that the maximum radial compressive stress is placed at the centre, immediately below the micro-particle; the maximum radial tensile stress occurs at the centre, within the coating and close to the interface. There are discontinuities at the layer interfaces. By introducing a multilayer structure (three-layer coating and five-layer coating), the maximum radial tensile stress decreases compared to that at the same location for single-layer coating (Fig. 4.2).

Fig. 4.3 (a) shows the normal stress distribution along the axial symmetry axis when loaded by a wear particle of 2.5 µm radius, in single-, three-, and five-layer DLC coatings. It is clear that a difference up to 8 GPa can be obtained between the single-layer coating and the five-layer coating in the models.

The same trend in normal radial stress distribution is shown in Fig. 4.3. It is clear that the maximum radial compressive stress is placed at the centre of the interface. The peak of the normal radial stress of the five-layer coating under the loading of 5 μm and 10 μm wear particle (Fig.4.3 (b) and (c)) are 9.85 GPa and 5.34 GPa, respectively, which are only 59% and 57% of that of the single-layer coating.

Fig.4.3 (d) shows the curve of the same depth of different wear particles (2.5μm, 5 μm, and 10 μm) in the coating. With the increase of the radius of wear particle from 2.5 μm to 10 μm, the maximum normal radial stress also increases, from 9.33 GPa to 20.21 GPa.

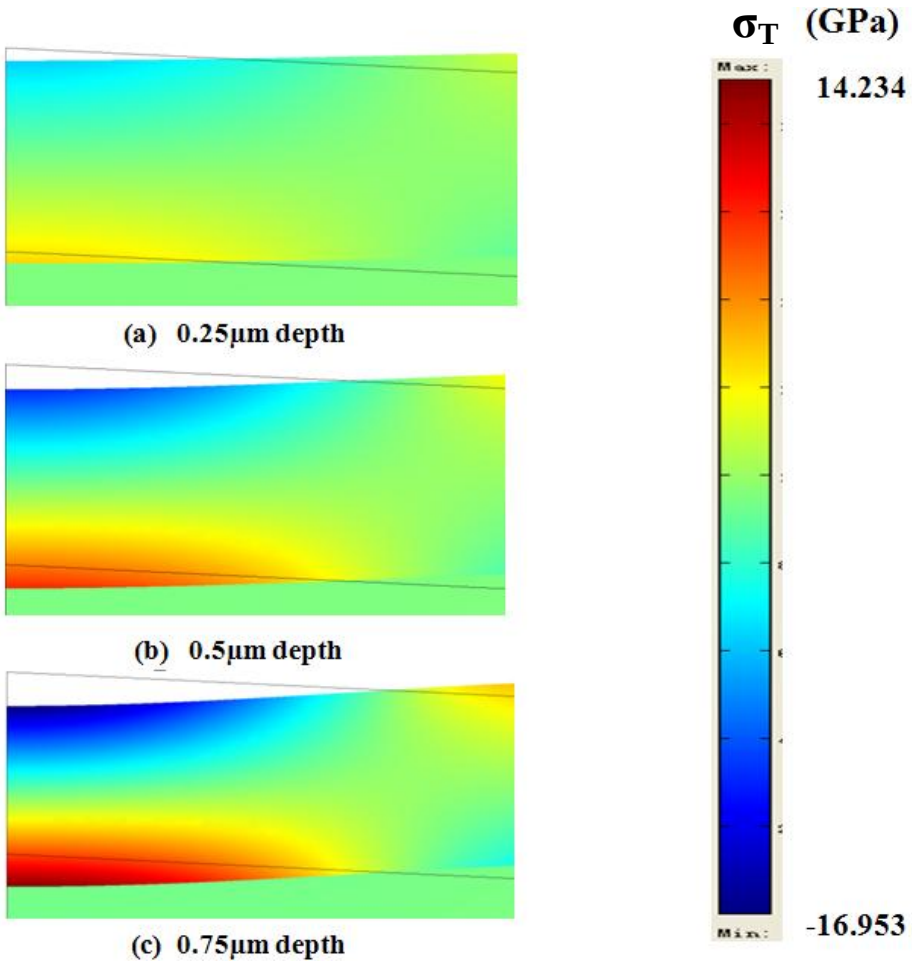

Fig. 4.4 Distribution of normal radial stress (σ_r) in the single-layer coating with an indentation depth of (a) 0.25 μm, (b) 0. 5 μm, and (c) 0.75 μm. The loading particle has a radius of 10 μm.

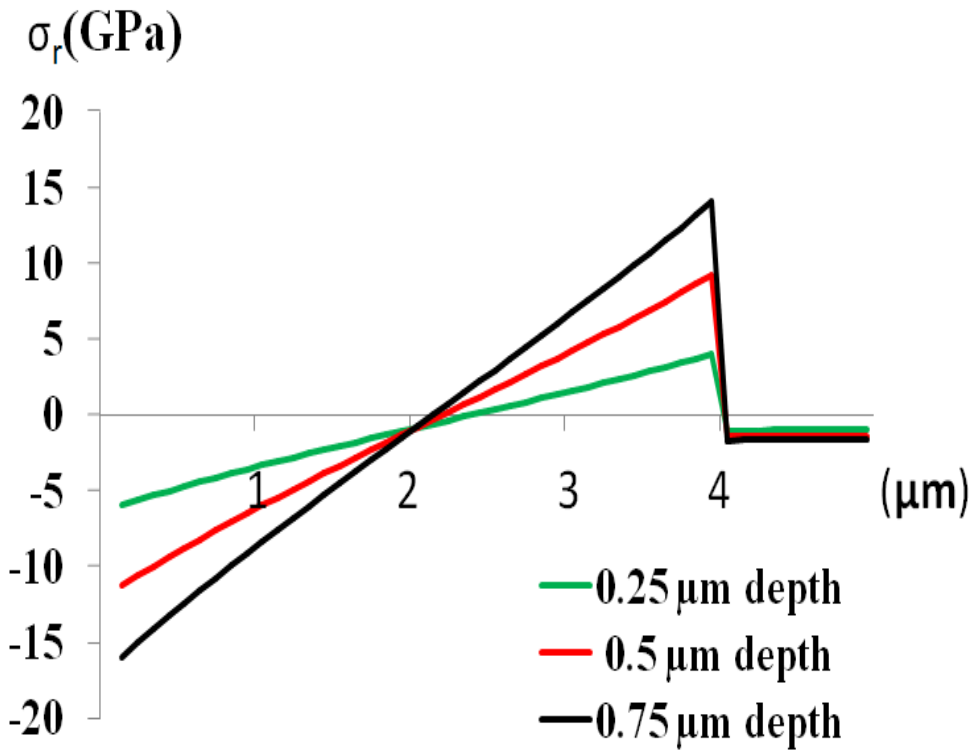

Fig. 4.5. The distribution of normal radial stress (σ_r) along the symmetry axis, in a monolithic coating layer and with different indentation depths

A comparison of distribution of normal radial stress (σ_r) between different indentation depths within the single-layer coating is shown in Fig. 4.4, the radius of the loading particle is 10 μm. From the picture, it is clear that the maximum values of normal radial stress are σ_r along the interface between the coating and substrate. The maximum normal radial stress under the loading of a 10 μm radius wear particle increases from 4.02 GPa to 14.24 GPa with the increase of the depth from 0.25 μm to 0.75 μm (Fig. 4.5).

Table 4.1 Maximum values of normal stress σ_r (GPa) along the coating (DLC) and substrate (CoCrMo) interface as a function of different indentation depth *h*.

Indentation depth, h (μm)	2.5μm radius of wear particle σ_r a			5μm radius of wear particle σ_r b			10μm radius of wear particle σ_r c		
	1 layer	3 layer	5 layer	1 layer	3 layer	5 layer	1 layer	3 layer	5 layer
0.25	9.68	6.29	5.52	8.05	5.19	4.53	4.02	2.45	2.07
0.5	20.21	13.59	12.05	16.61	11.14	9.85	9.33	6.12	5.34
0.75	29.96	20.40	18.15	24.38	16.57	14.71	14.24	9.57	8.40

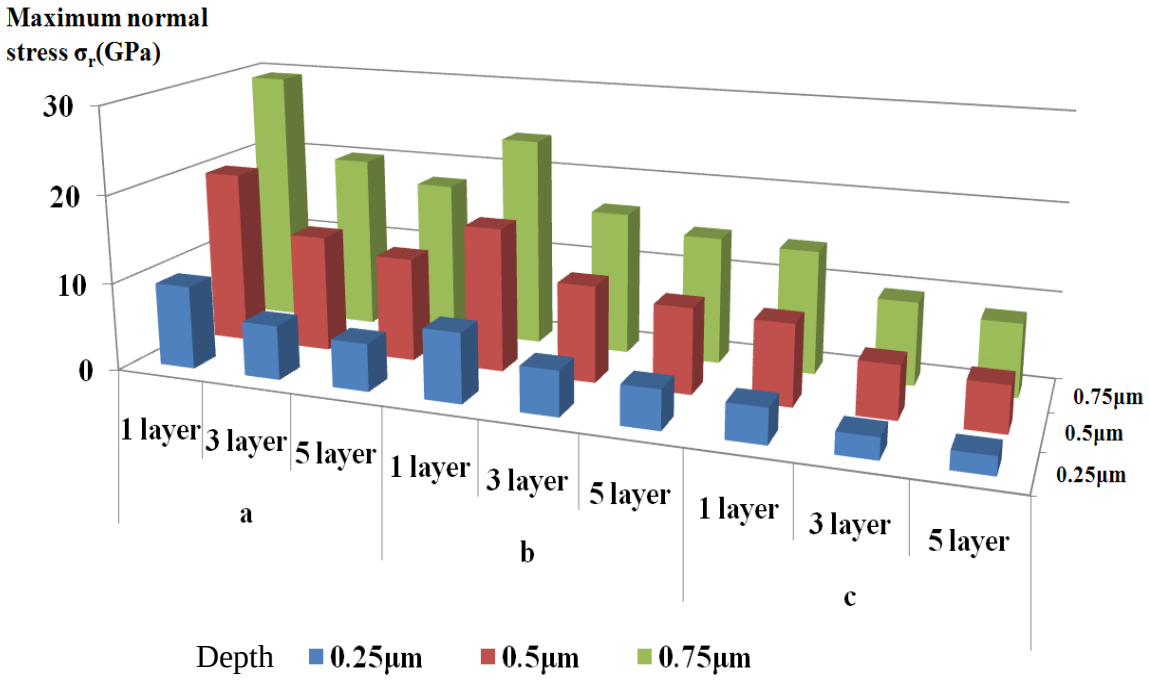

Fig. 4.6. Maximum normal radial stress σ_r (GPa) under the action of wear particle of different radius wear particle sizes: (a) 2.5 μm, (b) 5 μm, and (c)10 μm

Table 4.1 shows the maximum values of normal stress in all the DLC coatings modelled. A bar chart (Fig. 4.6) is presented, based on Table 4.1. From the bar chart, it can be seen that the maximum normal radial stress (29.96 GPa) occurs in the single-layer coating interface, with an indentation depth of 0.75 μm. The stress decreases with the increase of the number of the coating layers under the same loading conditions (indentation depth and particle size)..

4.22 Shear stress

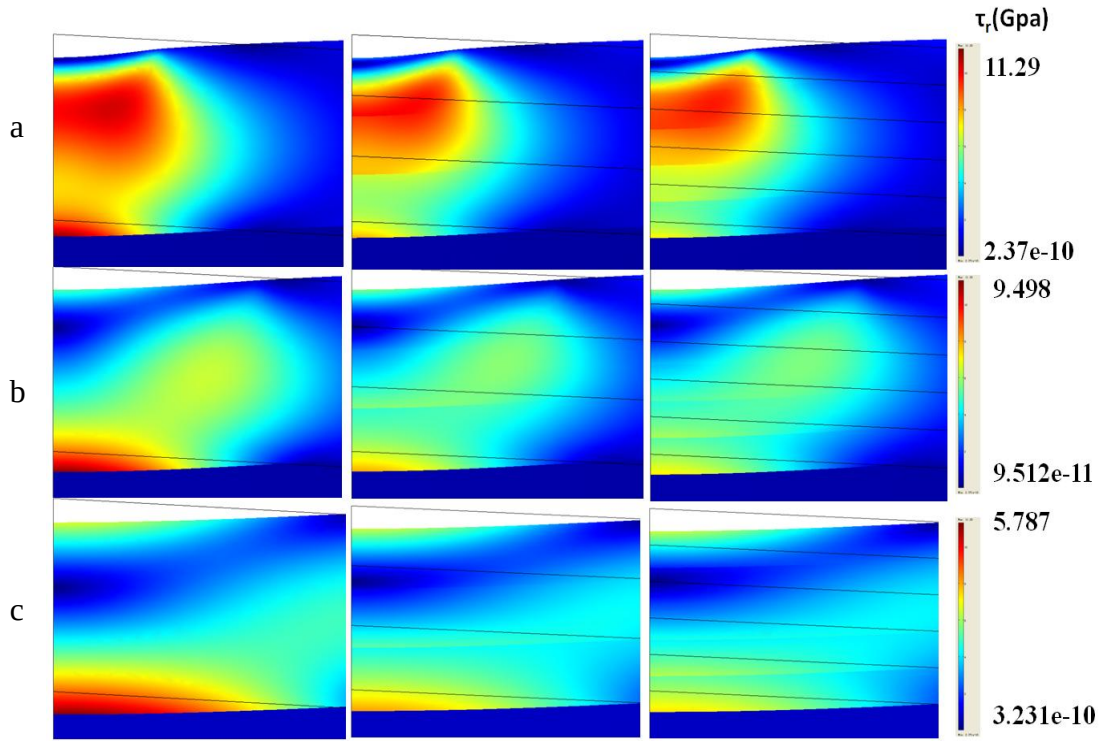

Fig. 4.7 Distribution of shear stress (τ_r) at an indentation depth of 0.5 μm, for loading particle with the radius of (a) 2.5 μm, (b) 5.0 μm, and (c) 10 μm.

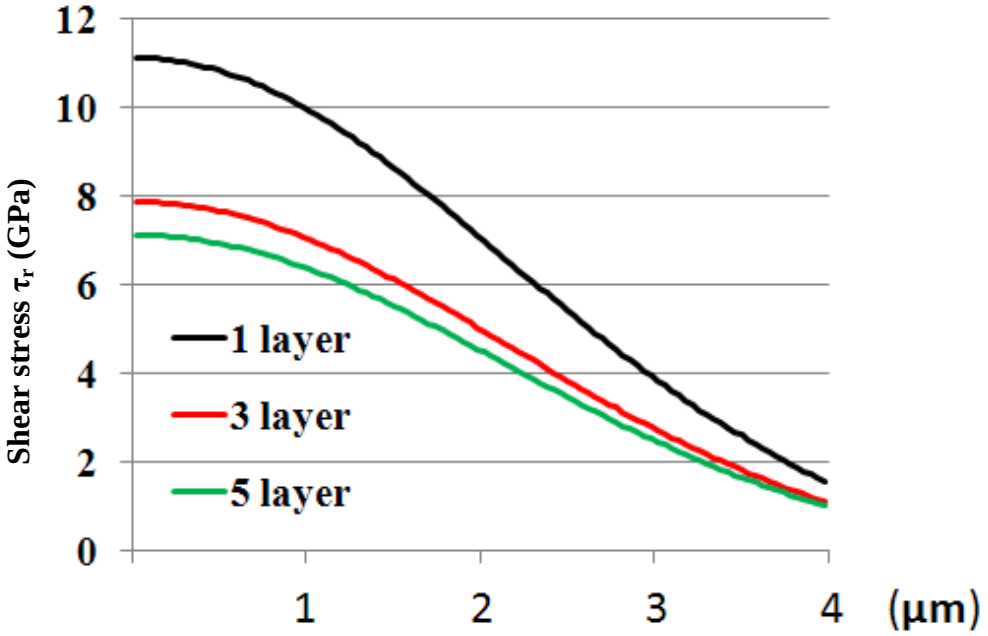

distance d (μm)

(a)

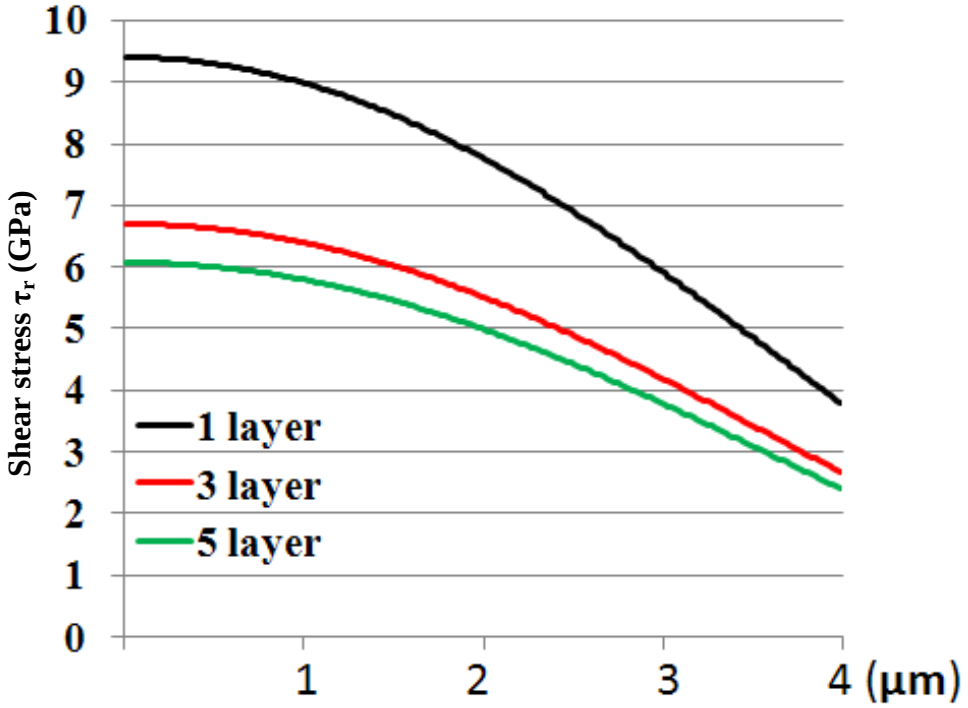

distance d (μm)

(b)

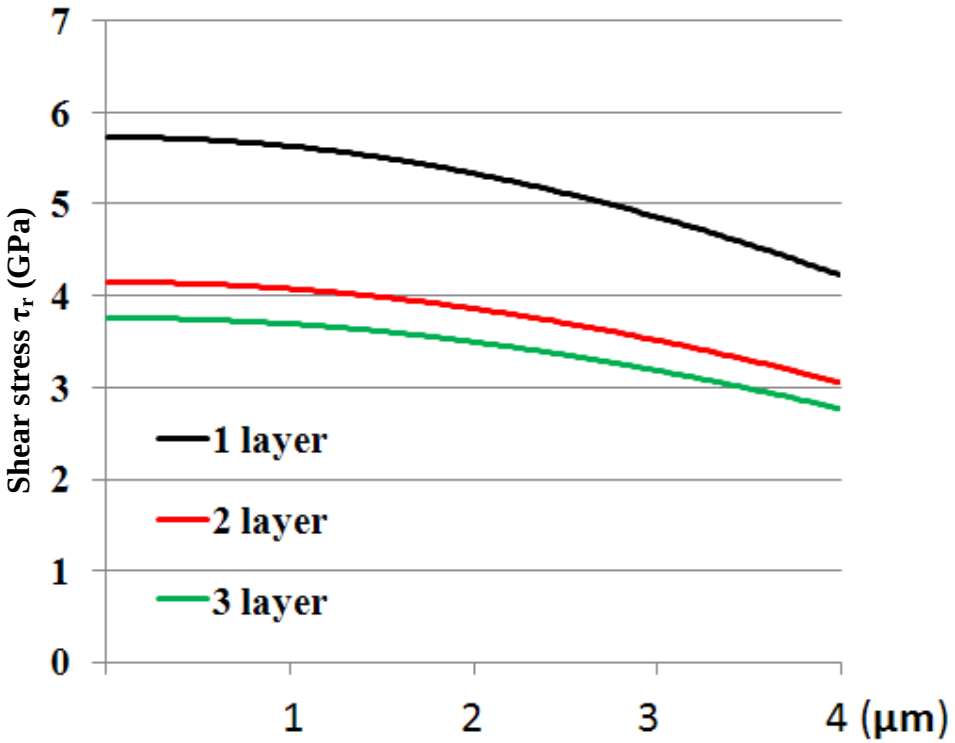

(c)

Fig. 4.8. Shear stress (τ_r) distributions, along the interface between the coating to substrate, towards positive r direction, for the loading particle with a radius of (a) 2.5 μm, (b) 5 μm, and (c) 10 μm. d is measured from r=0.

The distributions of the shear stress (τ_r) for different wear particle sizes are shown in Fig. 4.7. The location of the maximum shear stress changes with different systems. For the 2.5 μm radius loading particle (Fig. 4.7(a)), the maximum shear stress is above the interface between the coating and substrate, and below the surface of the coating, within the coating and close to the surface of the coating. Unlike the first line (Fig. 4.79(a)), the maximum shear stress is in the centre of the interface in the second line (Fig. 4.7(b)) and the third line (Fig. 4.7(c)). As expected, the maximum shear stress can be reduced with the increased number of coating layers.

Fig. 4.8(a) shows the effect of shear stress (τ_r) distribution on the interface under the loading of 2.5 μm radius wear particle for single, three, and five layers of coating. A reduction up to 3 GPa can be achieved when the number of layers is increased from one to five. The shear stress distributions of three different layers were also shown in the first line of the Fig. 4.7.

The same trend of varying of shear stress (τ_r) distribution can be observed in Fig. 4.8(b) and Fig. 4.8(c). The maximum shear stresses of the five-layer coating, under the loading of wear particles of 5 μm and 10 μm radius (Fig. 4.8(b) and (c)), are 6.12 GPa and 3.79 GPa, respectively， which are only 64% and 65% of the respective single-layer coatings.

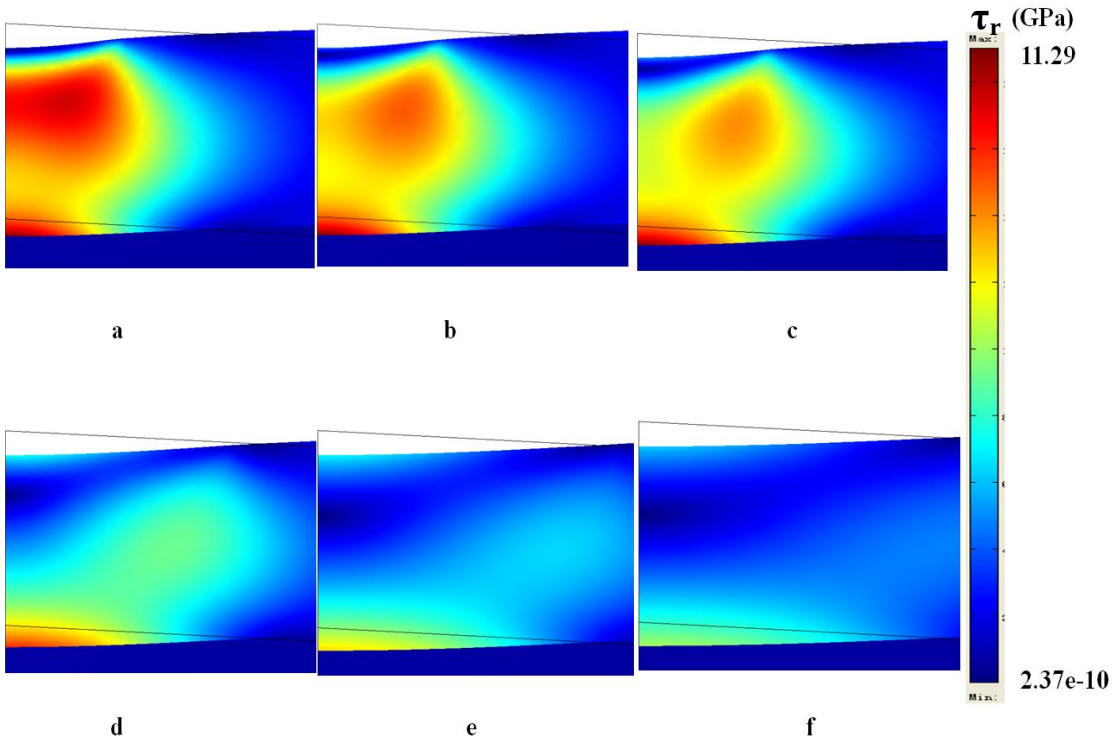

Fig. 4.9. The distribution of shear stress at 0.5 μm indentation depth, for different size of micro-particles with the radius of (a) 2.5 μm, (b) 2.8 μm, (c) 3 μm, (d) 5 μm, (e) 7 μm, and (f) 9 μm.

Fig. 4.9 shows the distribution of shear stress at 0.5 μm indentation depth, for different sizes of microparticles. The maximum shear stress moves downward as the particle becomes larger.

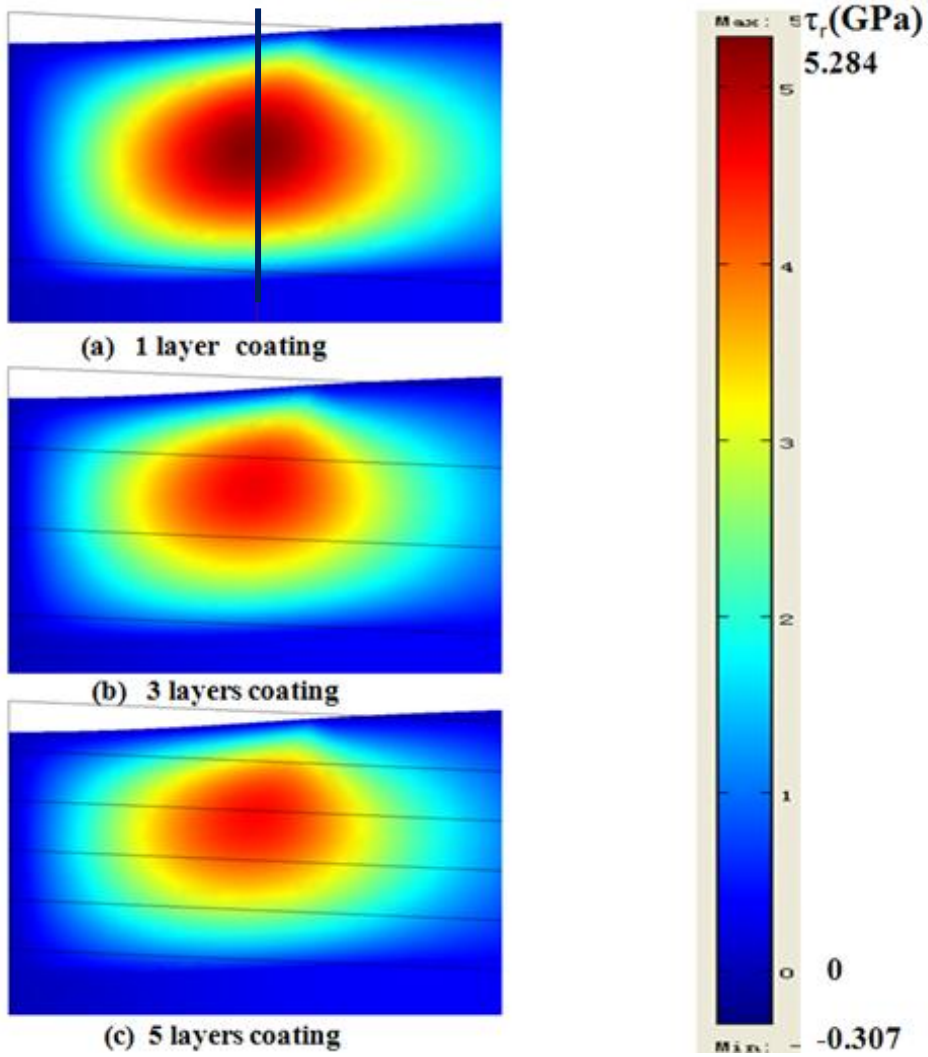

Fig. 4.10. Shear stress (τ_{rz}) distribution at an indentation depth of 0.5 μm under the loading of wear particle of 5μm radius: (a) single-layer coating, (b) three-layer coating, and (c) five-layer coating.

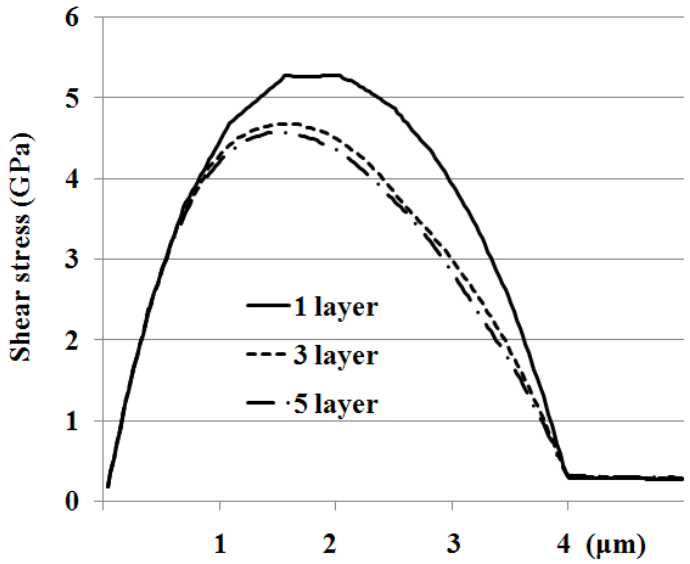

Fig. 4.11. Comparison of the maximum shear stress (τ_{rz_max}) along the black line in Fig 4.10(a), when loaded by a 5 µm radius microparticle. Distance d is measured from the coating surface downward

The distributions of the shear stress (τ_{rz_max}) along the black line in Fig 4.10(a), when loaded with a 5 µm radius microparticle, are shown in Fig. 4.10. The locations of the maximum shear stress are in the same position in the three different layered structures. It is above the interface, between the coating and substrate, and below the surface of the coating. As expected, the maximum shear stress can be reduced with the increase in the number of coating layers. A reduction in the maximum shear stress up to 1 GPa can be achieved by using the five-layer coating instead of the single-layer coating.

Table 4.2 Maximum shear stress τ_r (GPa) along the coating (DLC) and substrate (CoCrMo) interface under different indentation depths

Indentation depth, h(μm)	Maximum shear stress τ_r GPa, wear particle radius 2.5μm			Maximum shear stress τ_r GPa, wear particle radius 5μm			Maximum shear stress τ_r GPa, wear particle radius 10.0μm		
	1 layer	3 layers	5 layers	1 layer	3 layers	5 layers	1 layer	3 layers	5 layers
0.25	6.13	6.00	5.68	5.00	3.57	3.24	2.92	2.12	1.94
0.5	11.29	7.89	7.18	9.50	6.76	6.12	5.79	4.18	3.79
0.75	16.31	13.31	13.03	13.52	9.62	8.68	8.38	6.04	5.45

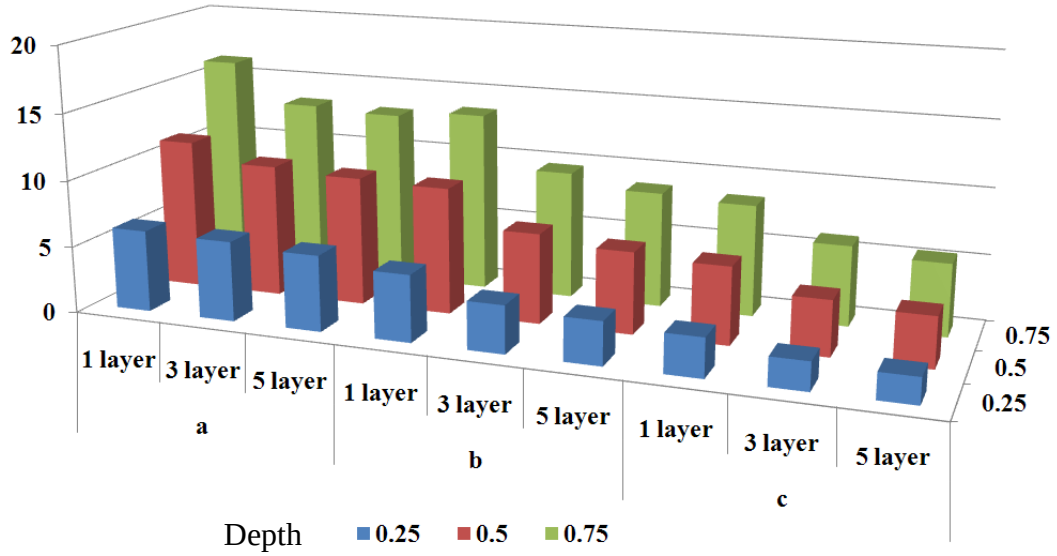

Fig. 4.12 The maximum shear stress τ_r (GPa) for wear particle with a radius of (a) 2.5 μm, (b) 5 μm, and (c) 10.0 μm.

Table 4.2 shows the maximum shear stress in all the coating systems and loading conditions. A bar chart is presented (Fig. 4.12), based on Table 4.2. The maximum shear stress of 16.31 GPa occurs in the single-layer coating under 0.75 μm indentation depth. Under different loading conditions (particle size and indentation depth), the shear stress level also decreases when the number of coating layers increases.

CHAPTER 5
DISCUSSION

5.1 Introduction

In artificial joints, delamination or failure within the coating occurs when stress reaches a critical level, resulting in large wear debris particles appearing on the contact surface between the head and the cup. The process has been described as due to a stress corrosion cracking mechanism (Falub et al., 2009). Under the same loading, stress increases when the contact area decreases, which happens in the vicinity of wear debris. As such, once wear debris is generated, a catastrophic process could be initiated, resulting in more stress corrosion cracking. As such, acquiring a strong coating that will not fail is highly desirable for the applications of hip joint replacement. Failure in a coating layer is normally initiated by excessive local tensile or shear stress; therefore, it is important to clarify the stress distribution within the coating layer under different loading conditions, which is necessary for improving the load-carrying capability of the coating. Unlike the previous studies, these filed, highly elastic modulus and hardness of the DLC multilayer coatings were presented in this work. Under normal contact conditions, plastic deformation occurs in contacting materials when the contact pressure is greater than the hardness of the materials (Singh et al., 2010). Therefore, high hardness coatings can resist plastic deformation to avoid failure of the coating; in addition, multilayer coatings can decrease stress concentration to avoid cracking. The purpose of this study , then, is to determine how the multilayer coatings improve the property of the coatings against potential cracks.

5.2 The region of stress distribution in single-layer coating

5.2.1 The region of normal stress distribution in single-layer coating

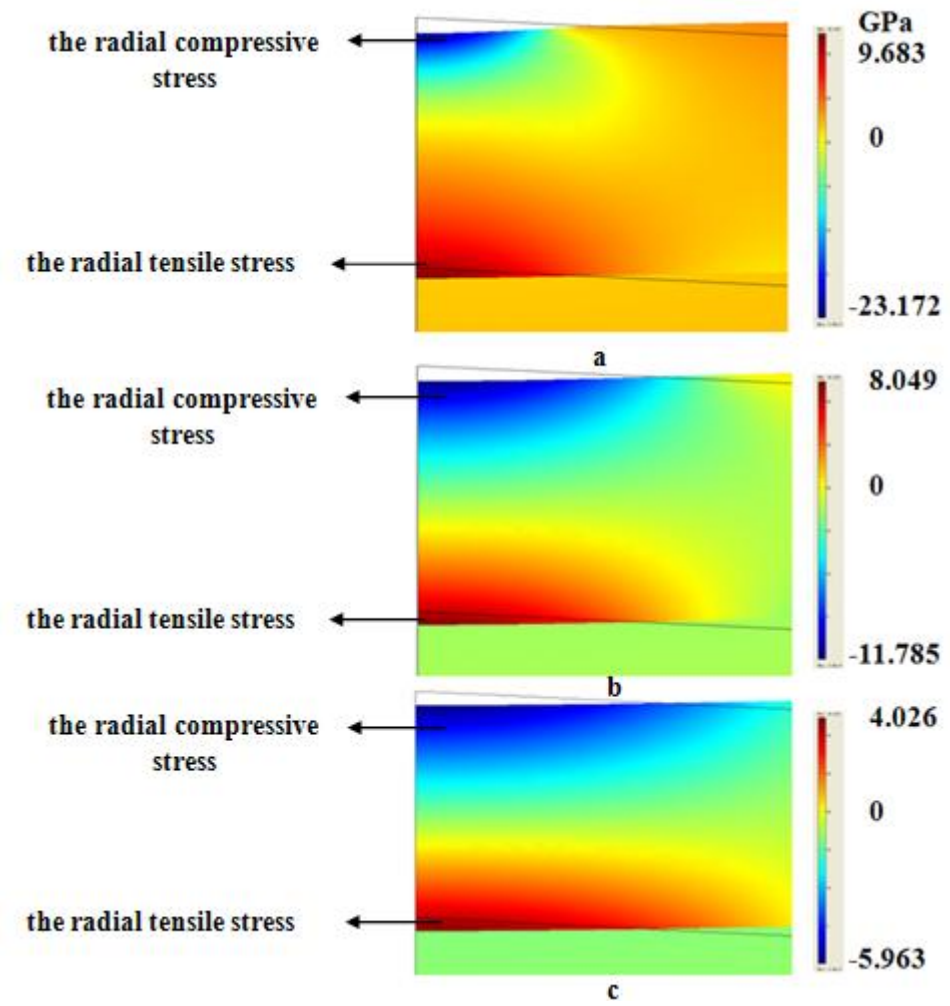

Fig.5.1 Locations of the radial tensile stress and the radial compressive stress at an indentation depth of 0.5 μm under the loading of different wear particles: (a) 2.5 μm radius, (b) 5.0 μm radius, and (c) 10 μm radius

The simulated normal stress distributions are shown in Fig. 5.1. The stress distributions have been created for DLC coatings with three different layers, in order to compare them between different structures of the coatings. The modelling of the stresses and strains in the surface can show the situation of the deformations clearly in the coating and substrate. Fig. 5.1 shows a region of very high maximum tensile stresses in the single-layer coating modelling, about the same size with the contact zone width under the contact surface. The maximum tensile stress region is concentrated at the centre of the interface. The regions of maximum tensile stresses increase as the size of wear particle increases. This is due to the big difference in Young's modulus between the DLC coating (500 GPa) and CoCrMo substrate (200 GPa). The maximum radial compressive stress is placed at the centre of the DLC

coating surface, immediately below the wear particle. Fig .5.1 shows a region of very high maximum compressive stresses in the single-layer coating, modelling about the same size, with the contact zone width under the contact surface. In the same situation as the maximum tensile stresses, the regions of maximum compressive stresses increase as the size of the wear particle increases. The maximum compressive stresses were affected more than the maximum tensile stresses as the size of wear particle varied from 2.5 μm to 10 μm. The maximum compressive stresses decreased from 23 GPa to 6 GPa, while the maximum tensile stresses decreased from 9.5 GPa to 4 GPa.

5.2.2 The region of the shear stress distribution in single-layer coating

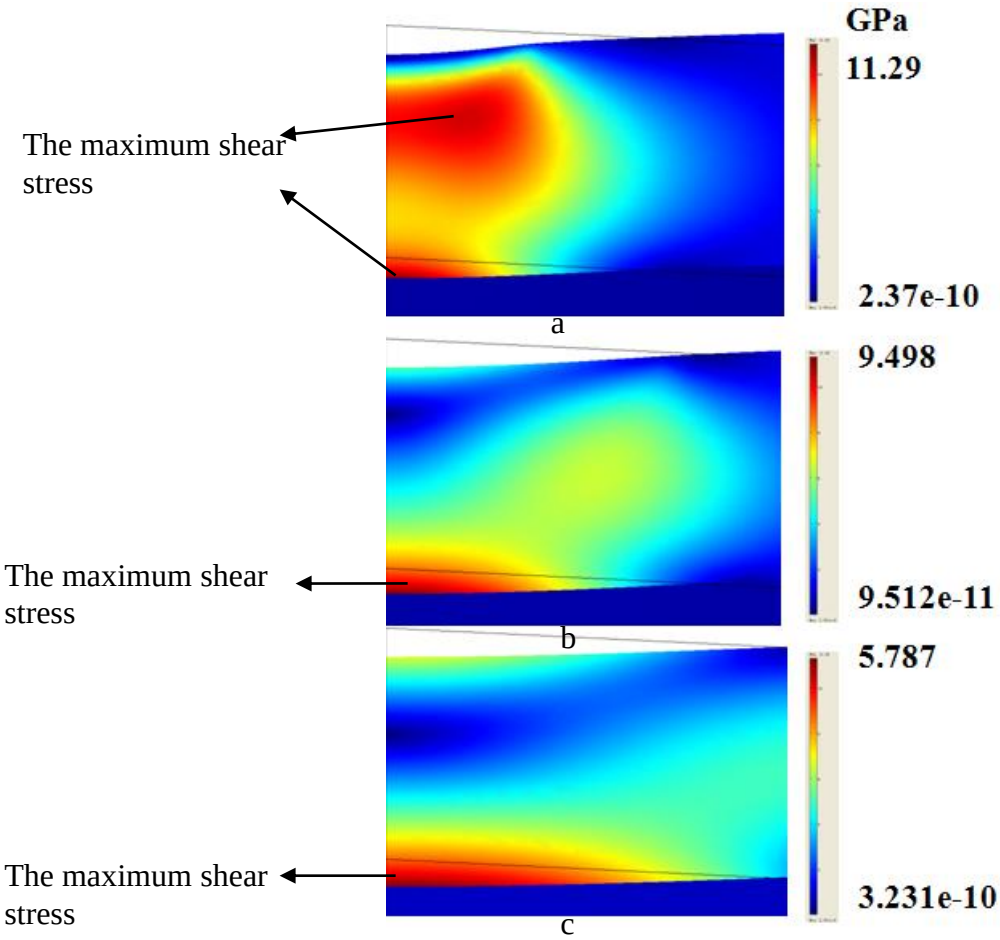

Fig. 5.2 Location of shear stressesan indentation depths of 0.5 μm under the loading of different wear particles: (a) 2.5 μm radius, (b) 5.0 μm radius, and (c) 10 μm radius

The simulated shear stress distributions are shown in Fig. 5.2. The modelling of the stresses and deformation in the surface can be seen clearly in the coating and substrate. Fig. 5.2(a) shows that the maximum shear stresses region is concentrated at both the centre of the DLC coating and the centre of the interface. However, in Fig. 5.2(b) and (c), the maximum shear stresses region only places in the centre of the interface. The regions of maximum shear stresses increase as the size of wear particle increases, while the magnitude of the maximum shear stresses decreases with increase of the size of wear particle size.

5.3 Region of stress distribution in three-layer and five-layer coatings

The stress distributions were created for coatings with three different layers in order to compare the different structures of the coatings. The modelling of the stresses and strains in the surface can show the situation of the deformations clearly in the coating and substrate (Fig. 4.2 and Fig. 4.7).

5.3.1 Normal stress distribution

The regions of maximum tensile stresses and maximum compressive stresses in three- and five-layer coatings is the same as single-layer coating. It is clear that the maximum tensile stresses located in the centre of the interface, and the maximum compressive stresses, are about the same size with the contact zone width under the contact surface. It can be seen that the value of the tensile stress at the coating-substrate interface is lower in the five-layer coating (12.05 GPa) and in three-layer coating (13.59 GPa) than that in the single- layer coating (20.21 GPa) (Fig. 4.3 (a)). As with single-layer coating, the tensile radial stress was distributed broadly in the radial direction across the interface in the three- and five-layer coatings. In addition, the tensile stress at the interfaces is higher (13.59 GPa) in the three-layer coating than in the five-layer coating (12.05 GPa). In other words, the difference between three-layer coating and five-layer coating is only 1 GPa, which means it is not a big influence for the coating property.

5.3.2 Shear stress distribution

For both the three-layer and five-layer coatings, very big changes in the maximum shear stresses in the centre of the interface are observed when comparing single-, three-, and five-layer coating stress distribution (Fig. 4.8). Unlike the single-layer coating, the maximum shear stresses region is only concentrated in the centre of the interface in three-layer and five-layer coatings. The influence of the young's modulus on stress distribution is obvious. It can be seen that the magnitude of the shear stress at the coating–substrate interface is lower in five-layer coating (7.89 GPa) and three-layer coating (7.18 GPa) than in single-layer coating (11.29 GPa) (Fig. 4.8(a)). In addition, the shear stress at the interfaces is higher (7.89 GPa) in three-layer coating than in five-layer coating (7.18 GPa). In other words, the difference between three-layer coating and five-layer coating is only 0.7 GPa. Thus, coating property has a small influence.

5.4 The Influence of Multiple-Layer Coatings

The hardness of the DLC coating on CoCrMo substrate can reach 43 GPa (Poliakov, Siqueira et al., 2004). The hardness of many materials is approximately three times its yield strength (Tabor, 1951), and the yield strength for the DLC coating is about 14 GPa. Table 4.2 shows the maximum values of shear stress in all the coatings. Fig.4.12 shows a bar chart based on Table 4.2. From the bar chart, it is clear the maximum shear stress occurs in the single-layer coating interface, and the peak (16.31 GPa) of the whole system occurs in 0.75 μm depth coating. The trend of the normal stress decreases with the increase in the number of the coating layers of the same depth and radius of wear particle. As the maximum shear stress (16.31 GPa) is higher than the yield strength (14 GPa), a crack might occur in the single-layer coating. The influence of the Young's modulus on the stress distribution is obvious. Multiple-layer coating can avoid this problem, as the maximum shear stress in three-layer coating (13.31 GPa) and five-layer coating (13.03 GPa) is lower than yield strength.

The simulation results showed that not only were the maximum stresses reduced, but also the stress distributions were modified, resulting in an overall reduction in the stress level throughout the coatings. According to the distribution of radial stress in the coatings, single-layer coating forms a radial crack before three-layer coating and five-layer coating (Fig. 4.2.). In the five-layer coating, the tensile radial stress was distributed broadly in the radial direction across the interface. This means the maximum tensile stress decreases with radial increase of the wear particles.

The maximum shear stress τ_{rz_max} moves to interface with a radial increase of the microparticle (Fig.4.10), which is consistent with the observation of Fig. 4.9.

5.5 The link between stress concentration and the initiation of cracks

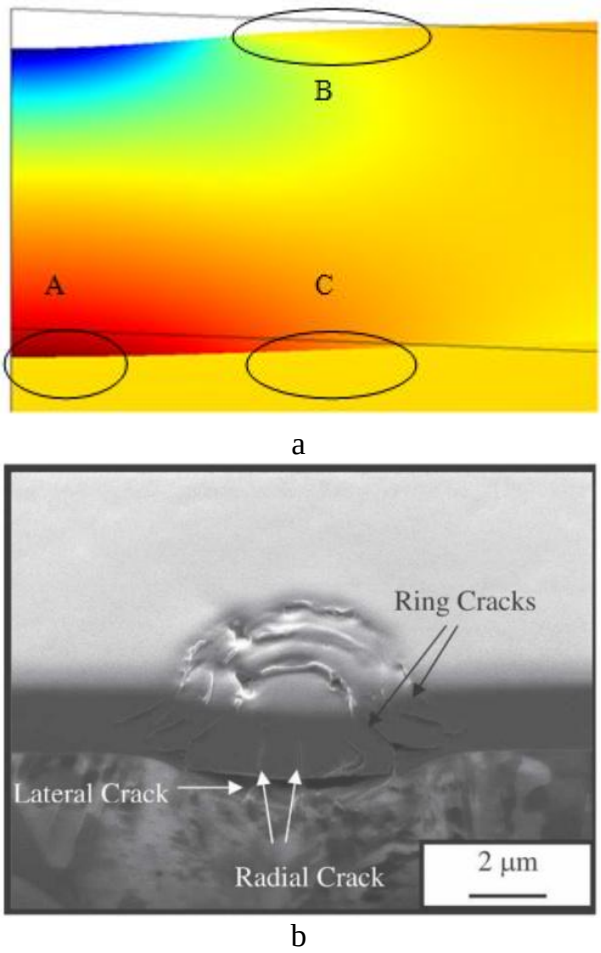

Fig. 5.3 (a) The simulated distribution of normal stress under indentation, (b) Indentation-induced damage to the DLC coating system (Singh et al., 2008)

Stress concentration plays a very important role in the initiation of cracks. There are three types of indentation cracks; radial, ring, and lateral cracks (Xie et al., 2007). Multilayer structures have been known as a design strategy to resist propagation of cracking (Mayer, 2005). However, the effect depends primarily on the details of the materials and structure being used. By understanding the stress distribution in the coating (Fig. 5.3), the multilayer structures can be tailored to lower the magnitude of stress and minimize the material volume it affects. In doing so, the load-bearing ability of the resultant coatings will be increased.

CHAPTER 6
SUMMARY AND CONCLUSIONS

6.1 Summary

To avoidance of failure of the head surface is one of the most challenging problems in hip joint replacement today. According to the previous studies, cracking is the main problem, and there are many reasons to help avoid cracks in the surface of the hip joint replacement. However, there are still some drawbacks; even the DLC coating is coated on the surface of the CoCrMo substrate, as the stress concentration always occurs at the interface. Improving the structure of the coating becomes necessary to change the property of the DLC coating. Unlike previous studies, the DLC multilayer coatings with high elastic modulus and hardness was presented in this work. Under normal contact conditions, plastic deformation appears in contacting materials when the contact pressure is greater than the hardness of the materials. Therefore, high hardness coating can resist the plastic deformation and avoid failure of the coating, while multilayer coatings can decrease the stress concentration to avoid cracking.

This thesis presents a review of experimental and FEM works carried out in the past. The methods adopted in the study of the hip joint replacement have been reviewed. In general, approaches to distribution analysis of stress in hip joint replacements are broadly categorised into two groups: experiment and Finite Element Method. These reviews have analysed the stress distribution of hip joints. It is very important to find an efficient way to improve the property of the coating. In terms of mapping the stress distribution in a new structure of the coating, the finite element modelling approach has more potential in simulating the hip joint replacement.

A ball-and-socket model was presented to simulate the metal-on-metal (MOM) hip joint replacement in this study. The DLC layers were deposited on the surface of a CoCrMo biomedical implant alloy. Three different structures of coating were

modelled in this work: single-layer coating, three-layer coating, and five-layer coating. All three coating systems have the same thickness—4 μm thick.

In an artificial joint, delamination or failure within the coating occurs when stress reaches a critical level, resulting in large wear debris particles that appear on the contact surface between the head and cup. Failure in a coating layer is normally initiated by excessive local tensile or shear stress; therefore, it is important to clarify the stress distribution within the coating layer under different loading conditions.

6.2 Conclusion

Based on the present study, the following general conclusions were drawn.

- Three different kinds of DLC multilayer coatings with highly elastic modulus and hardness were presented. All of the three coating systems have the same overall thickness, but the Young's modulus of different layers is not the same. The property of the coating can be improved not only as high hardness coating can resist the plastic deformation to avoid the failure of the coating, and multilayer coating can decrease stress concentration.

- The region of shear stress distribution in the single-layer coating has been studied. The maximum shear stress region is concentrated at the centre of the DLC coating and the centre of the interface. The region of very high maximum tensile stresses in the single-layer coating modelling is about the same size, with the contact zone width under the contact surface. The maximum tensile stress region is concentrated at the centre of the interface. In addition, the region of maximum compressive stresses places in the single-layer coating modelling is about the same size, with the contact zone width under the contact surface.

- The regions of maximum tensile stresses and maximum compressive stresses in the three-layer and five-layer coating are the same as single-layer coating. It is clear that the maximum tensile stresses located in the centre of

the interface and maximum compressive stresses are about the same size, with the contact zone width under the contact surface. Unlike single-layer coating, the maximum shear stress region is only concentrated at the centre of the interface in the three-layer and five-layer coatings. This can help avoid stress concentration in the interface.

- Maximum normal stress decreases with the increase of layers of coatings. This is expected to reduce the likelihood of ring cracks in these coatings.

- Maximum shear stress decreases with the increase of layers of coatings, which then reduces the probability of lateral cracks.

- Maximum normal stress and shear stress decrease with the increase of wear particles radius.

6.3 Recommendations for Future Work

The topic of the present work is one of the most important research topics in the predictive maintenance field. This area has good research potential, in view of the field requirements for the smooth operation of critical machinery and equipment. The approach of the current research work can be extended further to consider the following:

- Create three different coatings of the hip joint replacement with various depths.

- Create three different coatings of the hip joint replacement with various wear particles。

- Prepare experimentally different DLC multilayer coatings on CoCrMo alloy, then investigate the crack of the coatings under indentation and compare with the FEM results.

- Develop other materials as substrate to improve the property of the hip joint

replacement.

- Design and preparation of bias-graded DLC coatings by varying the bias voltage linearly during deposition.

- Study the adhesion, fatigue and wear properties of DLC coatings and analyse the corresponding failure mechanisms.

- Study the corrosion resistance of the DLC coatings on CoCrMo biomedical alloys.

REFERENCES

1. Igli. A., K.-I., V., Daniel M., Macek-Lebar A. (2002), Computer determination of contact stress distribution and size of weight bearing area in the human hip joint. *Computer Methods in Biomechanics and Biomedical Engineering*, Vol. 5, No.2, pp. 185–192.

2. Felson, D., et al. (2000). Osteoarthritis: new insights. Part 1: the disease and its risk factors. *Annals of Internal Medicine*, Vol.133, No.8, pp. 635.

3. Semlitsch, M. and H. Willert. (1997). Clinical wear behaviour of ultra-high molecular weight polyethylene cups paired with metal and ceramic ball heads in comparison to metal-on-metal pairings of hip joint replacements. P*roceedings of the Institution of Mechanical Engineers, Part H: Journal of Engineering in Medicine*, Vol.211, No.1, pp. 73-88.

4. Streicher, R., et al. (1996). Meta-on-metal articulation for artificial hip joints: laboratory study and clinical results. *ARCHIVE: Proceedings of the Institution of Mechanical Engineers, Part H: Journal of Engineering in Medicine 1989-1996 (vols 203-210)*, Vol. 210, No.38, pp. 223-232.

5. Walker, P. and B. Gold. (1971). The tribology (friction, lubrication and wear) of all-metal artificial hip joints. *Wear*, Vol.17, No. 4, pp. 285-299.

6. Amstutz, H., P. Grigoris, and F. Dorey. (1998). Evolution and future of surface replacement of the hip. *Journal of Orthopaedic Science*, Vol. 3, No. 3, pp. 169-186.

7. McMinn, D., et al. (1996). Metal on metal surface replacement of the hip: experience of the McMinn prosthesis. *Clinical orthopaedics and related Research*, Vol. 329, pp. S89.

8. Wagner, H. (1978). Surface replacement arthroplasty of the hip. *Clinical Orthopaedics and Related Research*, Vol.134, pp. 102.

9. Wagner, M. and H. Wagner. (1996). Preliminary results of uncemented metal on metal stemmed and resurfacing hip replacement arthroplasty. *Clinical Orthopaedics and Related Research*, Vol. 329, No. pp. S78.

10. Schmalzried, T., et al. (1996). Metal on metal surface replacement of the hip: technique, fixation, and early results. *Clinical orthopaedics and related research*, Vol329, pp. S106.

11. Jakobsen, S.S., et al. (2010). Biomechanical implant fixation of CoCrMo coating inferior to titanium coating in a canine implant model. *Journal of Biomedical Materials Research Part A*, Vol. 94, No.1, pp. 180-186.

12. Poliakov, V., et al. (2004). Physical and tribological properties of hard amorphous DLC films deposited on different substrates. *Diamond and Related Materials*, Vol.13, No.4, pp. 1511-1515.

13. Huang, N., et al. (2003). Hemocompatibility of titanium oxide films. *Biomaterials*, Vol. 24, No.13, pp. 2177-2187.

14. Shah, A., et al. (1999). High-resolution morphometric analysis of human osteoblastic cell adhesion on clinically relevant orthopedic alloys. *Bone*, Vol. 24, No. 5, pp. 499-506.

15. Falub, C.V., et al. (2009). A quantitative in vitro method to predict the adhesion lifetime of diamond-like carbon thin films on biomedical implants. *Acta Biomaterialia*, Vol. 5, No.8, pp. 3086-3097.

16. Faulhaber, S., et al. (2006). Buckling delamination in compressed multilayers on curved substrates with accompanying ridge cracks. *Journal of the Mechanics and Physics of Solids*, Vol. 54, No. 5, pp. 1004-1028.

17. Kim, H.J., et al. (2007). Observation of the failure mechanism for diamond-like carbon film on stainless steel under tensile loading. *Scripta Materialia*, Vol. 57, No.11, pp. 1016-1019.

18. Singh, R.K., et al. (2010). Design of functionally graded carbon coatings against contact damage. *Thin Solid Films*, Vol. 518, No. 20, pp. 5769-5776.

19. Reed, L., et al. (2000). The Effect of Femoral Component Head Size on Posterior Dislocation of the Artificial Hip Joint*. *The Journal of Bone and Joint Surgery (American)*, Vol. 82, No.9, pp. 1300-1300.

20. Cosmi, F., et al. 2006. A finite element method comparison of wear in two metal-on-metal total hip prostheses. *Proceedings of the Institution of Mechanical Engineers, Part H: Journal of Engineering in Medicine*, Vol.220, No. 8, pp. 871.

21. Schwarz, C., et al. (2008). Investigation on wear and adhesion of graded Si/SiC/DLC coatings deposited by plasma-enhanced-CVD. *Diamond and related materials*, Vol.17, No.7-10, pp. 1685-1688.

22. Ward, M., et al. (2010). Microscopical analysis of synovial fluid wear debris from failing CoCr hip prostheses. *IOP Publishing*.

23. Tipper, J., et al. (2000). Quantitative analysis of polyethylene wear debris, wear rate and head damage in retrieved Charnley hip prostheses. *Journal of Materials Science: Materials in Medicine*, Vol. 11, No. 2, pp. 117-124.

24. Wong, P., F. He, and X. Zhou. (2010). Interpretation of the hardness of worn DLC particles using micro-Raman spectroscopy. *Tribology International*, Vol. 43, No. 10, pp. 1806-1810.

25. Harris, W.H. (1994). Osteolysis and particle disease in hip replacement: a review. *Acta Orthopaedica*, Vol. 65, No. 1, pp. 113-123.

26. Koseki, H., et al. (2008). Surface-engineered metal-on-metal bearings improve the friction and wear properties of local area contact in total joint arthroplasty. *Surface and Coatings Technology*, Vol. 202, No. 19, pp. 4775-4779.

27. Bolelli, G., et al. (2011). Wear and corrosion behaviour of HVOF WC-CoCr/CVD DLC hybrid coating systems deposited onto aluminium substrate. *Surface and Coatings Technology*, Vol. 205, pp. 4211-4220.

28. Cui, F. and D. Li. (2000). A review of investigations on biocompatibility of diamond-like carbon and carbon nitride films. *Surface and Coatings Technology*, Vol. 131, No.1, pp. 481-487.

29. Thorwarth, G., et al. (2010). Tribological behavior of DLC-coated articulating joint implants. *Acta Biomaterialia*, Vol. 6, No.6, pp. 2335-2341.

30. Gillespie, W., et al. (1988). The incidence of cancer following total hip replacement. *Journal of Bone and Joint Surgery-British Volume,* Vol. 70, No. 4, pp. 539.

31. Cui, F. and Z. Luo. (1999). Biomaterials modification by ion-beam processing. *Surface and Coatings Technology*, Vol. 112, No. 1-3, pp. 278-285.

32. Tipper, J., et al. (1999). Quantitative analysis of the wear and wear debris from low and high carbon content cobalt chrome alloys used in metal on metal total hip replacements. *Journal of Materials Science: Materials in Medicine*, Vol. 10, No.6, pp. 353-362.

33. Wang, A., A. Essner, and R. Klein. (2001). Effect of contact stress on friction and wear of ultra-high molecular weight polyethylene in total hip replacement. *Proceedings of the Institution of Mechanical Engineers, Part H: Journal of Engineering in Medicine*, Vol. 215, No. 2, pp. 133-139.

34. Anderson, A.E., et al. (2008). Validation of finite element predictions of cartilage contact pressure in the human hip joint. *Journal of Biomechanical Engineering*, Vol.130, No.05, pp. 1008.

35. Rapperport, D., D. Carter, and D. Schurman. (1985). *Contact finite element stress analysis of the hip joint. Journal of orthopaedic research*, vol. 3, No. 4, pp. 435-446.

36. Cilingir, A.C. (2010). Finite element analysis of the contact mechanics of ceramic-on-ceramic hip resurfacing prostheses. *Journal of Bionic Engineering*, Vol. 7, No. 3, pp. 244-253.

37. Sfantos, G. and M. Aliabadi. (2007). Total hip arthroplasty wear simulation using the boundary element method. *Journal of biomechanics*, Vol, 40. No. 2, pp. 378-389.

38. Liu, H., et al. (2010). Coupling of dynamics and contact mechanics of artificial hip joints in a pendulum model. *Proceedings of the Institution of*

Mechanical Engineers, Part H: Journal of Engineering in Medicine, Vol. 224, No. 8, pp. 989-1003.

39. Kang, L., et al. (2009). Enhanced computational prediction of polyethylene wear in hip joints by incorporating cross-shear and contact pressure in additional to load and sliding distance: Effect of head diameter. *Journal of biomechanics*, Vol.42, No. 7, pp. 912-918.

40. Bachtar, F., X. Chen, and T. Hisada, (2006). Finite element contact analysis of the hip joint. *Medical and Biological Engineering and Computing*, Vol. 44, No. 8, pp. 643-651.

41. Kluess, D., et al. (2007). Influence of femoral head size on impingement, dislocation and stress distribution in total hip replacement. *Medical Engineering and Physics*, Vol. 29, No.4, pp. 465-471.

42. Cruz, R., et al. (2006). DLC-ceramic multilayers for automotive applications. *Diamond and related materials*, Vol. 15, No.11-12, pp. 2055-2060.

43. Deng, J. and M. Braun. (1995). DLC multilayer coatings for wear protection. Diamond and related materials, Vol. 4, No, 7, pp. 936-943.

44. Zhang, X., et al. (2006). Modeling of thermal residual stresses in multilayer coatings with graded properties and compositions. *Thin Solid Films*, Vol. 497, No. 1, pp. 223-231.

45. Bentzon, M., C. Barholm-Hansen, and J.B. Hansen. (1995). Interfacial shear strength of diamond-like carbon coatings deposited on metals. *Diamond and related materials*, Vol. 4, No. 5, pp. 787-790.

46. Nir, D. (1987). Intrinsic stress in diamond-like carbon films and its dependence on deposition parameters. *Thin Solid Films*, Vol. 146, No.1, pp. 27-43.

47. Zhao, X., Z. Xie, and P. Munroe. (2011). Nanoindentation of hard multilayer coatings: Finite element modelling. *Materials Science and Engineering: A*, Vol. 528, No. 3, pp. 1111-1116.

48. Singh, R.K., et al. (2008). Contact damage evolution in diamondlike carbon coatings on ductile substrates. Journal of Materials Research, Vol. 23, No. 01, pp. 27-36.

49. Gao, L., et al. (2009). Effect of 3D physiological loading and motion on elastohydrodynamic lubrication of metal-on-metal total hip replacements. *Medical engineering & physics*, Vol. 31, No. 6, pp. 720-729.

50. Falub, C., et al. (2011). In vitro studies of the adhesion of diamond-like carbon thin films on CoCrMo biomedical implant alloy. *Acta Materialia*, Vol. 59, No. 11, pp. 1359-6454.

51. Oliver, W.C. and G.M. Pharr. (1992). Improved technique for determining hardness and elastic modulus using load and displacement sensing

indentation experiments. *Journal of Materials Research*, Vol. 7, No. 6, pp. 1564-1583.

52. Xie, Z.H., et al. (2007). Contact damage evolution in a diamond-like carbon (DLC) coating on a stainless steel substrate. *Thin Solid Films*, Vol. 515, No. 6, pp. 3196-3201.

53. Abdul-Baqi, A. and E. Van der Giessen. (2001). Indentation-induced interface delamination of a strong film on a ductile substrate. *Thin Folid Films*, Vol. 381, No. 1, pp. 143-154.

54. Tabor, D. (1951). The hardness of metals. *Oxford University Press*.

55. Mayer, G. (2005). Rigid biological systems as models for synthetic composites. Science, Vol. 310, No. 5751, pp. 1144.